Derivation of flow and transport parameters from outcropping sediments of the Neogene aquifer, Belgium.

Bart ROGIERS[1,2], Koen BEERTEN[1], Tuur SMEEKENS[2], Dirk MALLANTS[3], Matej GEDEON[1], Marijke HUYSMANS[2,4], Okke BATELAAN[2,4,5] & Alain DASSARGUES[2,6]

[1] Institute for Environment, Health and Safety, Belgian Nuclear Research Centre (SCK•CEN), Boeretang 200, BE-2400 Mol, Belgium.
[2] Dept. of Earth and Environmental Sciences, KU Leuven, Celestijnenlaan 200e - bus 2410, BE-3001 Heverlee, Belgium.
[3] Groundwater Hydrology Program, CSIRO Land and Water, Waite Road - Gate 4, Glen Osmond SA 5064, Australia.
[4] Dept. of Hydrology and Hydraulic Engineering, Vrije Universiteit Brussel, Pleinlaan 2, BE-1050 Brussels, Belgium.
[5] School of the Environment, Flinders University, GPO Box 2100, Adelaide SA 5001, Australia.
[6] Hydrogeology and Environmental Geology, Dept. of Architecture, Geology, Environment and Civil Engineering (ArGEnCo) and Aquapole, Université de Liège, B.52/3 Sart-Tilman, BE-4000 Liège, Belgium.

ABSTRACT. Centimetre-scale saturated hydraulic conductivities (K) are derived from air permeability measurements on a selection of outcrops of the Neogene aquifer in the Campine area, Belgium. Outcrop sediments are of Miocene to Quaternary age and have a marine to continental origin. Grain size analyses for the same outcrops and corresponding K predictions using previously developed models are also presented. We discuss outcrop hydrogeological properties and quantify the heterogeneity within the outcrops in detail using geostatistical variography. Moreover, outcrop-scale K values, their anisotropy and dispersivities are numerically calculated as a means to upscale such small-scale measurements to a larger scale commensurate with the scale of flow and transport modelling. By studying the small-scale variability as observed in outcrops, we gain crucial understanding of the larger-scale behaviour of the corresponding hydrogeological units within the Neogene aquifer, the most important groundwater reservoir of Flanders. The results of this study will equally improve conceptual hydrogeological model building and parameterization.

KEYWORDS: Air permeameter, grain size, spatial variability, upscaling, anisotropy, dispersivity

1. Introduction

The Neogene aquifer underlying the Campine area in northeast Belgium (Fig. 1) is considered to be the most important groundwater reservoir in Flanders, with drinking water production exceeding 120×10^6 m³/yr (VMM, 2005). It underlies both the Scheldt and Meuse river basins and consists of Oligocene (Rupelian) to Mio-Pliocene sediments with a Quaternary cover (Fig. 2). The main lithologies include fine to medium grained, glauconitic, micaceous sands with Fe sandstone layers and lignite layers. A varying clay content is found in certain units (e.g. Kasterlee, Poederlee, Lillo and Diest Formations), while basal gravels are present between the units (Laga et al., 2001). Deposition took place in a shallow marine to perimarine environment at the southern margin of the North Sea Basin (Louwye et al., 2007; Louwye & Laga, 2008; Louwye & De Schepper, 2010). The Quaternary deposits have various textures and thicknesses and unconformably overlie the Neogene units and constitute the upper part of the aquifer system (not shown on Fig. 2); the Boom Clay aquitard forms the lower boundary of the aquifer (see e.g. Yu et al., 2012).

Groundwater recharge mainly occurs on the elevated regions of the Campine Plateau and the cuesta of the Campine Complex (Fig. 1), and the numerous smaller interfluvia distributed across the study area. Groundwater abstraction, pollution by diffuse sources including agriculture, former metallurgic industry (Seuntjens et al., 2002), coal mines and point sources are the main stresses on both groundwater quantity and quality (Coetsiers

et al., 2008). Hydrodynamic evolution of the aquifer since 1833 was studied by Van Camp et al. (2010), and groundwater chemistry was investigated by Coetsiers & Walraevens (2006). Groundwater abstraction happens mostly via deep wells in the Formations of Diest and Berchem to avoid use of lower quality shallow groundwater polluted by surface activities; it represents about 12% of the estimated aquifer recharge (Van Camp et al. 2012).

Patyn et al. (1989) concluded from hydrogeological assessments that all sediments above the Boom Clay behave as a single aquifer, despite the lithological differences between the different aquifer units. More recent investigations however resulted in an update of the hydrogeological classification (Meyus et al., 2000; VMM, 2008) and in correspondingly more refined groundwater models (Gedeon et al., 2007; Gedeon, 2008; Gedeon & Mallants, 2012). Model updating involved abandoning the concept of a single aquifer in favour of using two aquifers separated by a retarding layer: the Kasterlee Clay aquitard. From 2008-2010, the hydrogeological characterization of the different units within this aquifer has been further intensified in the framework of developing a surface repository for low and intermediate level short-lived radioactive waste (ONDRAF/NIRAS, 2010). The investigations included a few hundred cone penetration tests (Rogiers et al., 2010a-c), eight cored boreholes in the Mol/Dessel region and numerous lab analyses (Beerten et al., 2010). This new information resulted in refining the hydrogeological models (Gedeon et al., 2011; Gedeon & Mallants, 2012; Rogiers
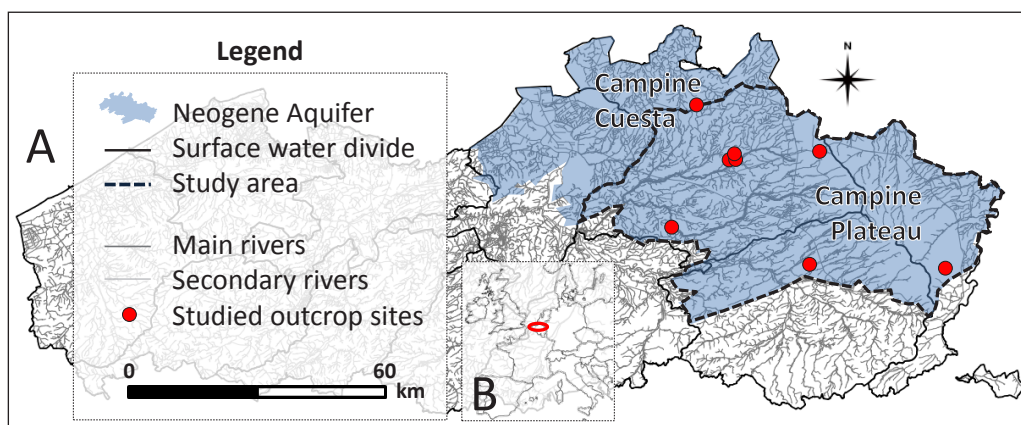

Figure 1. A: Location of the outcrop sites and the study area within the Neogene aquifer, in Flanders, Belgium. B: Location of Flanders within Europe.
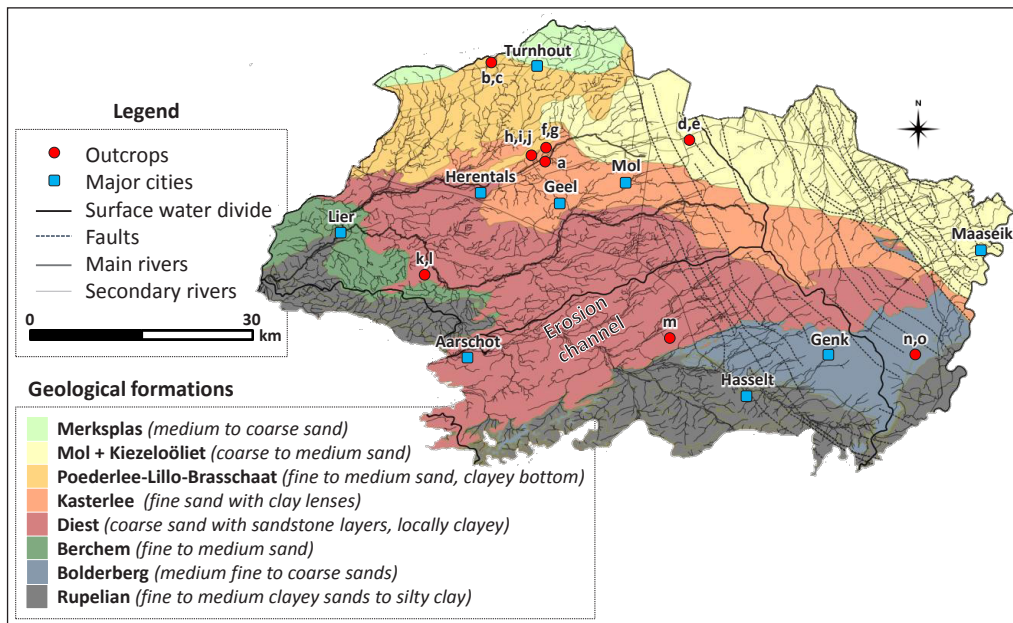
Figure 2. Geological map of the Tertiary formations within the studied part of the Neogene aquifer, with the selected outcrop sites and several major cities.

et al., 2010a) and included quantifying the influence of small-scale (centimetre- to meter-scale) variability within the Neogene Aquifer (Rogiers et al., 2010b-d, 2011, 2012,2013a). Upscaling of such small-scale heterogeneity is key to building successful models at the larger, more practical scales typical of groundwater management models (Koltermann & Gorelick, 1996; De Marsily et al., 2005; Huysmans & Dassargues, 2009; Ronayne et al., 2010).

Using outcrop sediments as analogues for aquifer sediments is especially useful for characterizing such small-scale spatial variability in hydrodynamic properties (Huysmans et al., 2008; Possemiers et al., 2012; Rogiers et al., 2013a). Rogiers et al. (2013b) demonstrated the benefit of outcrop-based hydraulic conductivity estimates and their spatial variability for an improved understanding and quantification of an aquifer's heterogeneity in *K*. This paper presents a follow-up analysis of the Rogiers et al. (2013a,b) study and includes additional outcrop sediments while we also quantify a key contaminant transport parameter (i.e. dispersivity). To increase knowledge on the small-scale variability within the Neogene aquifer sediments, this paper presents detailed descriptions of 15 outcrops including grain size characteristics and several different hydraulic conductivity estimates. *K*-estimates include those based on i) grain size distributions using the predictive models of Rogiers et al. (2012), and ii) in-situ air permeameter measurements at the centimetre scale and their numerically calculated outcrop-scale equivalent values following the methodology of Rogiers et al. (2013a). Finally, we estimate the outcrop-scale dispersivity using an equivalent 2D uniform random walk approach (see Salamon et al., 2006).

2. Methods

2.1. Outcrop selection

The selection of outcrops was driven by two factors: 1) the need for outcrops analogues to those sediments that play a key role in the groundwater flow and transport modelling that underpin the safety assessment of the ONDRAF/NIRAS surface disposal project (ONDRAF/NIRAS, 2010), and 2) the need for natural analogues of engineered earth covers as part of a design study in which understanding the long-term behaviour of such systems is critical (Jacques et al. 2010). For this purpose, eight locations were selected within the study area (Figs 1 & 2), resulting in a total of 15 outcrops.

2.2. Estimation of hydraulic conductivity

2.2.1. Prediction from grain size

Grain size analyses were performed on outcrop sediments as a means to compare outcrops with subsurface sediments

(see Rogiers et al., 2013b); a further objective was to provide saturated hydraulic conductivity estimates independent of the air permeameter values. Grain size analyses were performed by laser diffraction using a Malvern Mastersizer (Malvern Instruments Ltd., UK). The method consists of monitoring the amount of reflection and diffraction that is transmitted back from a laser beam directed at the particles. Prior to analysis, 15g of each sample was dried at 60°C during at least 24h and aggregate-forming material like carbonate cements, organic material and Fe-oxides and hydroxides were removed. Each sample was then divided into 10 sub-samples by a rotary sample splitter to enable repeated measurements on a single sample, and all samples were measured at least twice. The final result was based on the average grain size distribution of all sub-samples. Note that particle sizes are expressed as size of an equivalent sphere with an identical diffraction pattern.

Various approaches exist to relate *K* to grain size data. Most methods use a single grain size parameter and hence omit the information encompassed by the entire grain size distribution. Rogiers et al. (2012) compared two data-driven modelling methods that use the entire grain size distribution data as input for prediction of *K*, i.e. multiple linear regression (MLR) and artificial neural networks (ANNs). Besides the predictive capacity of the methods, the uncertainty associated with the model predictions was also evaluated, since such information is important for stochastic groundwater flow and contaminant transport modelling. The ANN method was therefore combined with a generalized likelihood uncertainty estimation (GLUE) approach to predict *K* from grain size data. The resulting *K*-models were shown to be superior to non site-specific literature-based prediction models, including several of the models discussed by Vienken and Dietrich (2011) and the predictive *K* model of the Rosetta software (Schaap et al., 2001). The GLUE-ANN ensemble prediction also proved to be slightly better than the MLR model, and the prediction uncertainty was reduced by half an order of magnitude on average. Since the data used to develop the predictive *K*-models all originated from an area within the current study area, the same models are used in this paper to provide estimates of hydraulic conductivity. Since the superiority of site-specific calibrations was demonstrated (Rogiers et al., 2012), other non site-specific estimates are omitted. It should be noted however that some of the outcrop sediments display grain size fractions not previously observed in the aquifer sediments. Using the MLR model for such grain sizes would not introduce large errors; the non-linear GLUE-ANN model however might provide erroneous estimates for grain size distributions that were not used during model calibration ("training" of the ANNs).

2.2.2. Air permeameter-based measurements of hydraulic conductivity at the cm-scale

Centimetre-scale air permeameter measurements were performed with the Tinyperm II device (New England Research & Vindum Engineering, 2011). The device had an inner tip diameter of 9 mm, resulting in a depth of investigation between 9 and 18 mm, allowing for a very detailed small-scale analysis. The calibration was adjusted after fitting a filter into the device tip, as presented by Huysmans et al. (2008). The transfer function proposed by Iversen et al. (2003) was used to derive hydraulic conductivity estimates; validation of the approach based on laboratory-derived K-values on similar outcrop core samples was reported by Rogiers et al. (2013a).

2.2.3. Upscaling from cm-scale to outcrop-scale

Where it was possible to measure K on regular 2D grids on the outcrop faces, the numerical upscaling approach by Rogiers et al. (2013a) and Li et al. (2011) was applied to calculate outcrop-scale K values. This consists of creating 2D groundwater flow models whose numerical grids correspond to the measurement grids, with a set of artificial boundary conditions, and calculating a single equivalent K tensor for the entire domain by using the average fluxes and head gradients. Processing Modflow (Chiang & Kinzelbach, 2001) was used for this purpose. If measurements were made only along a single depth profile, arithmetic and harmonic means were calculated instead to obtain an outcrop-scale representative value. In one single case, several measurements were scattered over a large outcrop; geostatistical simulation was used to provide a grid for upscaling to outcrop-scale representative values.

2.3. Estimation of outcrop-scale dispersivity

The degree of mixing of chemicals in groundwater in the direction of groundwater flow (longitudinal dispersion) and transverse to the main flow direction (transverse dispersion) may be calculated on the basis of the longitudinal (α_L) and transverse dispersivity (α_T) and the porewater velocity v, e.g. $D_L = \alpha_L \times v$. In this paper particle tracking was used to derive α_L and α_T based

on the artificial boundary condition setups used to upscale the air permeameter measurements. Fig. 3 shows, as an example, the different boundary conditions that were applied to the Kasterlee Sands outcrop (vertical cross-section corresponding to the measurement grid at the outcrop face). Effects of heterogeneity in K on calculated heads, flow vectors, and particle pathlines are displayed for the different boundary conditions.

We used an equivalent 2D uniform random walk (Salamon et al., 2006) to describe the arrival times and locations of particles at the downgradient side of both permeameter-type setup simulations; the following equations describe the particle positions in the system (for the horizontal flow case):

$$x_p^k = x_p^{k-1} + v_x \Delta t + \sqrt{2D_L \Delta t} X_L$$

$$z_v^k = z_v^{k-1} + \sqrt{2D_T \Delta t} X_T$$

with x_p^k the x coordinate of particle p at timestep k, v_x the average velocity, Δt the time step, D_L and D_T the longitudinal and transversal dispersion coefficients, and X_L and X_T two independent random numbers from a standard normal distribution. Reordering these equations, and normalizing by the time to travel to the downgradient side of the flow model, for each individual particle, gives the following normal distributions with standard deviation

$$\frac{x_p^k - x_p^{k-1} - v_x \Delta t}{\sqrt{\Delta t}} = \sqrt{2D_L} X_L$$

$$\frac{z_p^k - z_p^{k-1}}{\sqrt{\Delta t}} = \sqrt{2D_T} X_T$$

The quantities on the left side can easily be obtained from the forward particle tracking end points. The standard deviations of
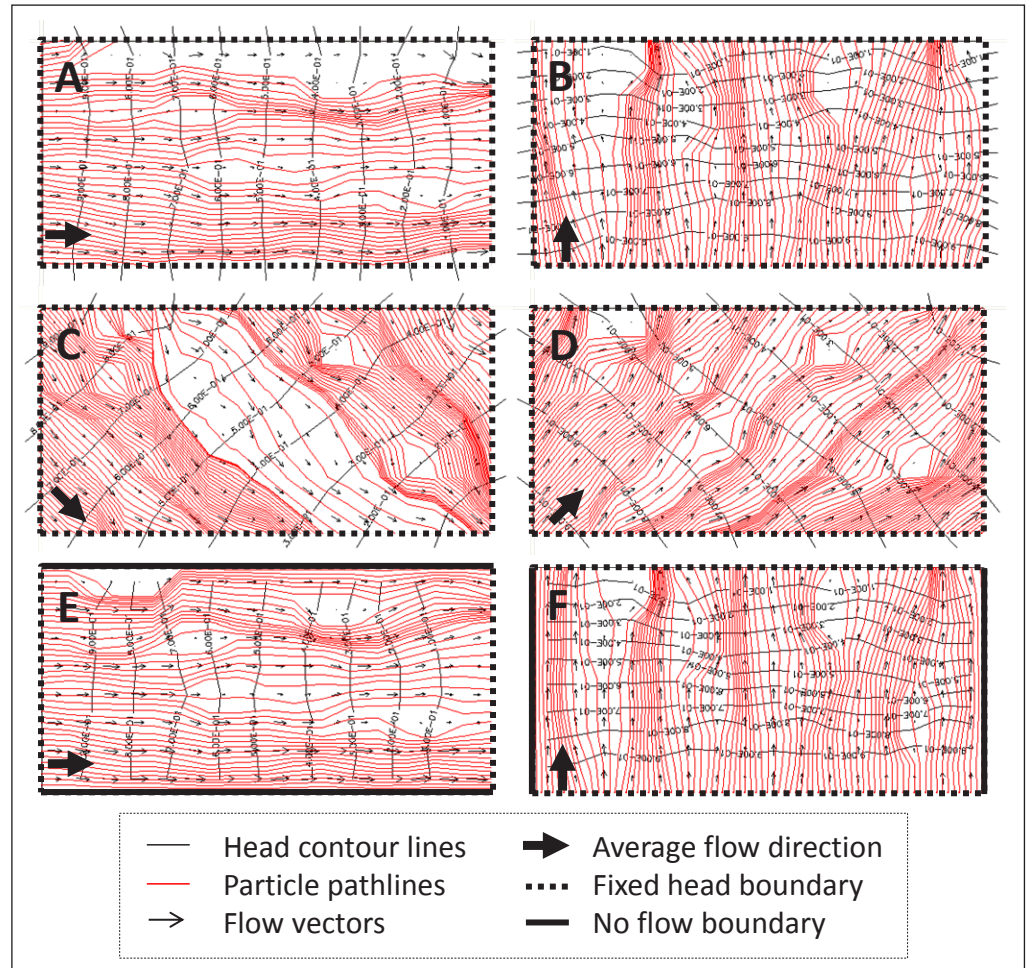

Figure 3. Particle tracking simulations for the Kasterlee Sands outcrop. A: horizontal flow setup, B: vertical flow setup, C, D: diagonal flow setup, E, F: horizontal and vertical permeameter-type setup. The modelled vertical cross-section represents the measurement grid at the outcrop face, with one grid cell for each obtained air permeability measurement.
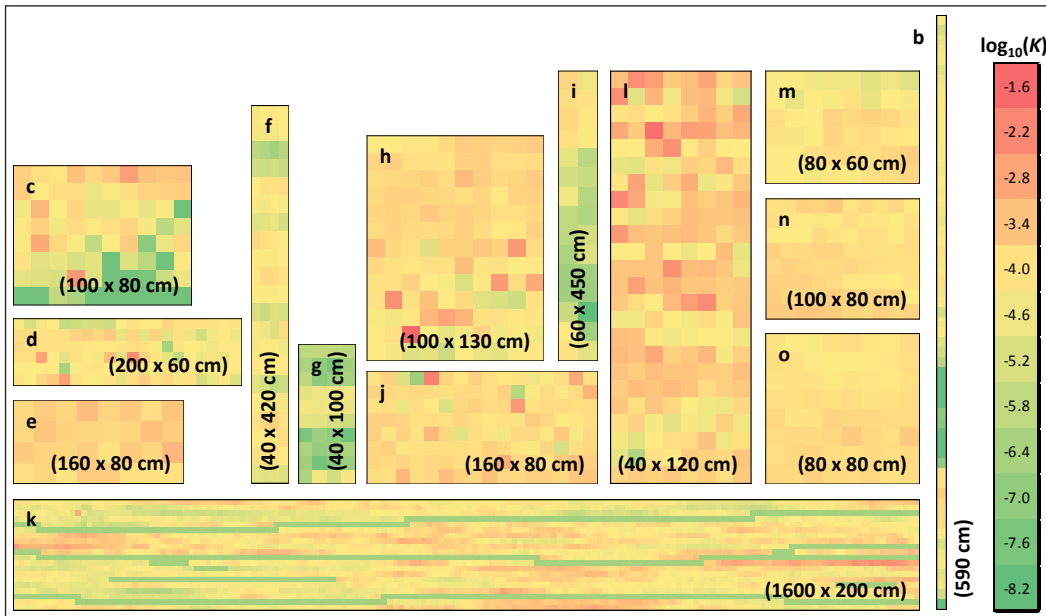
— Head contour lines   ➡ Average flow direction
— Particle pathlines   ···· Fixed head boundary
→ Flow vectors   ▬ No flow boundary

Figure 4. Overview of the air-permeability derived *K*-values for all outcrops; data grids used for numerically upscaling *K*-values. Grid k (Kasterlee Clay) is the only outcrop where geostatistical simulation is used for filling in missing values.

these are then used to estimate both D_L and D_T, and based on the average velocity v_x the dispersivities α_L and α_T are determined as $\alpha_L = D_L / v_x$ and $\alpha_T = D_T / v_x$.

Using the results of the particle tracking, outcrop-scale longitudinal and transversal dispersivity values can thus be calculated, both for horizontal and vertical flow, using the flow matrices from the *K* upscaling simulations. The estimated dispersivities are representative for the outcrop scales (at most several m travel distance), for larger travel distances a dispersion-scale relationship has to be invoked (Gelhar et al., 1992; Schulze-Makuch, 2005). The obtained values are representative for relatively short travel distances (a few m); they further can be added to an existing data set to build better dispersion-scale relationships, and can be used to extrapolate the obtained dispersivities towards the scale of interest.

3. Overview of the outcrop results

Outcrop sediments were investigated at 8 different locations, resulting in a total of 15 outcrops covering 11 different geological formations (see overview in Table 1). In addition to in-situ air permeability measurements, grain size data were collected

ID	Location	Stratigraphy	Age	# k_{air}	# gs	Upscaling
a	Kasterlee	Kleine Nete deposits	Quaternary	34	5	-
b	Beerse	Campine Clay-Sand Complex		58	27	Arithmetic and Harmonic means
c				80	-	
d	Lommel	Lommel Sands		182	-	
e		Mol Sands		32	-	
f	Kasterlee	Poederlee Sands	Pliocene	84	2	
g				40	1	Numerical upscaling using flow models and different boundary condition setups
h				130	-	
i	Lichtaart	Poederlee-Kasterlee transition zone		29	12	
j		Kasterlee Sands	Miocene	112	-	
k	Heist-op-den-berg	Kasterlee Clay		127	7	
l		Diest Clayey Top		192	4	
m	Lummen	Diest Sands		48	-	
n	Maasmechelen	Bolderberg Sands		80	-	
o				64	-	
			Total=	**1292**	**58**	

Table 1. Overview of the studied outcrops, number (#) of measurements (k_{air}: in-situ air permeability; gs: grain size), and upscaling approach.
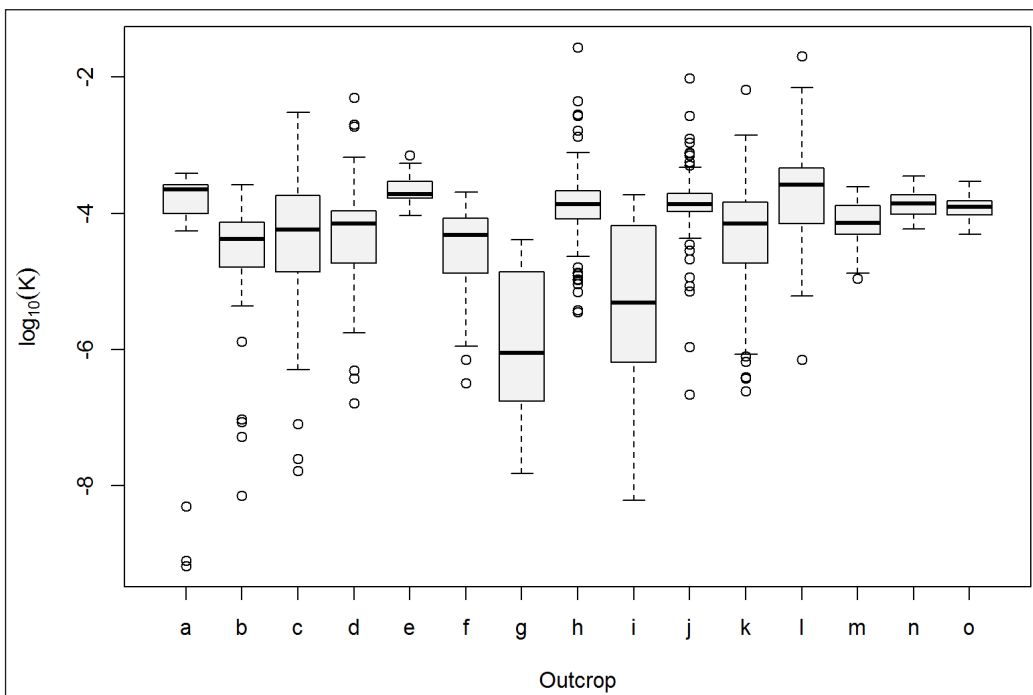

Figure 5. Boxplots of the air permeability-derived *K* values for 15 outcrops (see Table 2 for outcrop codes a-o).

| ID | | Stratigraphy | # k_{air} | Geomean K (m/s) | -log$_{10}$(K) | | | | | |
					Min	Mean	Max	Range	SD	CV
a	point bar sands	Kleine Nete deposits	31	1,88E-04	-4,26	-3,72	-3,41	0,84	0,24	-6%
	channel beds		3	1,39E-09	-9,17	-8,86	-8,3	0,87	0,48	-5%
b		Campine Clay-Sand	58	2,20E-05	-8,14	-4,66	-3,59	4,55	0,92	-20%
c		Complex	80	4,00E-05	-7,78	-4,4	-2,52	5,25	1,02	-23%
d		Lommel Sands	182	6,16E-05	-6,42	-4,21	-2,31	4,12	0,59	-14%
e		Mol Sands	32	2,10E-04	-4,04	-3,68	-3,15	0,89	0,22	-6%
f		Poederlee Sands	84	3,13E-05	-6,5	-4,5	-3,69	2,81	0,61	-14%
g			40	1,15E-06	-7,82	-5,94	-4,39	3,43	1,07	-18%
h			130	1,26E-04	-5,45	-3,9	-1,56	3,88	0,53	-14%
i		Poederlee-Kasterlee transition zone	29	5,20E-06	-8,21	-5,28	-3,73	4,48	1,14	-22%
j		Kasterlee Sands	112	1,33E-04	-6,66	-3,88	-2,01	4,64	0,5	-13%
k		Kasterlee Clay	127	4,24E-05	-6,61	-4,37	-2,19	4,42	0,82	-19%
l		Diest Clayey Top	192	2,08E-04	-6,15	-3,68	-1,69	4,45	0,64	-17%
m		Diest Sands	48	7,23E-05	-4,95	-4,14	-3,62	1,34	0,32	-8%
n		Bolderberg Sands	80	1,38E-04	-4,23	-3,86	-3,45	0,77	0,19	-5%
o			64	1,21E-04	-4,31	-3,92	-3,53	0,79	0,15	-4%
Total			**1292**							

Table 2. Extreme values (Min, Max), mean, range, standard deviation (SD), and coefficient of variation (CV) of log$_{10}$-transformed hydraulic conductivity K for all outcrops based on air permeability measurements (k_{air}).

for a subset of the sampling locations. An overview of the K-transformed air permeability measurements is presented in Fig. 4; subsequent sections provide a discussion of the geological formations and their corresponding outcrops on a one by one basis.

Descriptive statistics of all hydraulic conductivity values obtained from air permeameter measurements are given in Table 2. Heterogeneity in K is discussed on the basis of the mean and standard deviation (SD) of log$_{10}$-transformed hydraulic conductivity, minimum and maximum values, range (max - min) and the geometric coefficient of variation ($CV=100 \times SD/Mean$). The corresponding boxplots are given in Fig. 5. Not all sampling schemes were unbiased as the number of very low K values typical of fine-textured layers is underrepresented in some cases due to a very long measurement time or high moisture content. Regardless of these limitations of the measurement technique, considering

all outcrop data, a reasonable composite picture of the different sediments within the heterogeneous aquifer is obtained.

By repeating measurements on multiple samples, with log$_{10}$K between -3.5 and -6.5, the measurement error was determined to correspond to a geometric CV of about 2% (absolute value taken). The variability observed within each outcrop exceeds the variability owing to measurement error (Table 2). This indicates that the observed variability is mainly due to the sediment characteristics. For the second Bolderberg Sands outcrop (o), the measurement error may be up to half of the observed variability. Overall the measurement error is very small; hence it is not further treated separately.

Since the measurements of most outcrops were performed on regular grids with knowledge of the relative 2D coordinates, experimental variograms were calculated to describe the spatial structure within these outcrops. Outcrop a was omitted as no
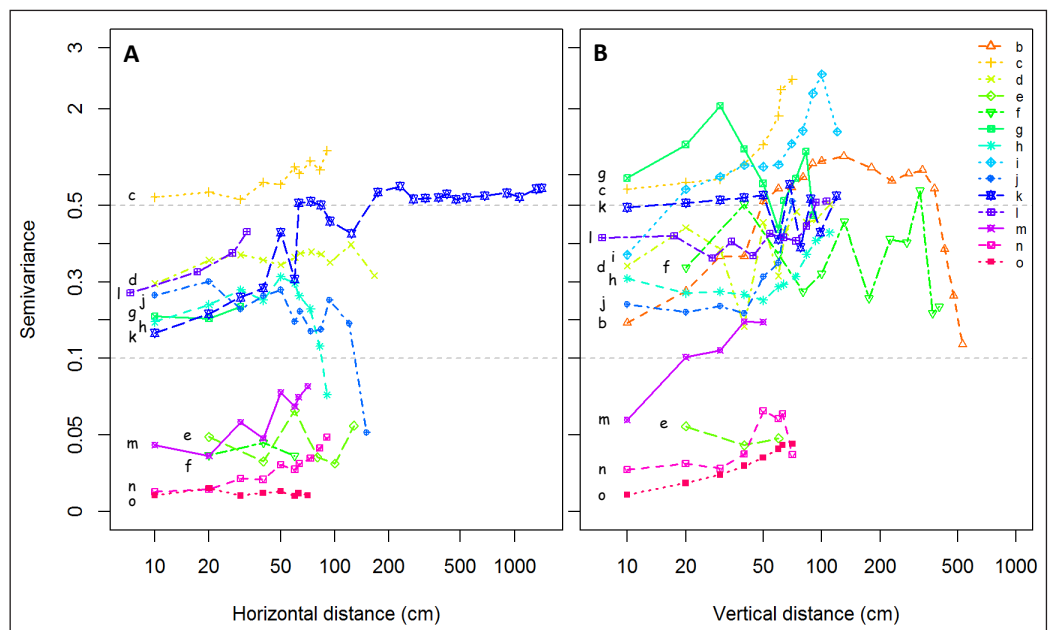

Figure 6. Directional (A: horizontal; B: vertical) experimental variograms for the outcrops (see Table 2 for outcrop codes a-o). Note the y-axis is a stack of three different scales.
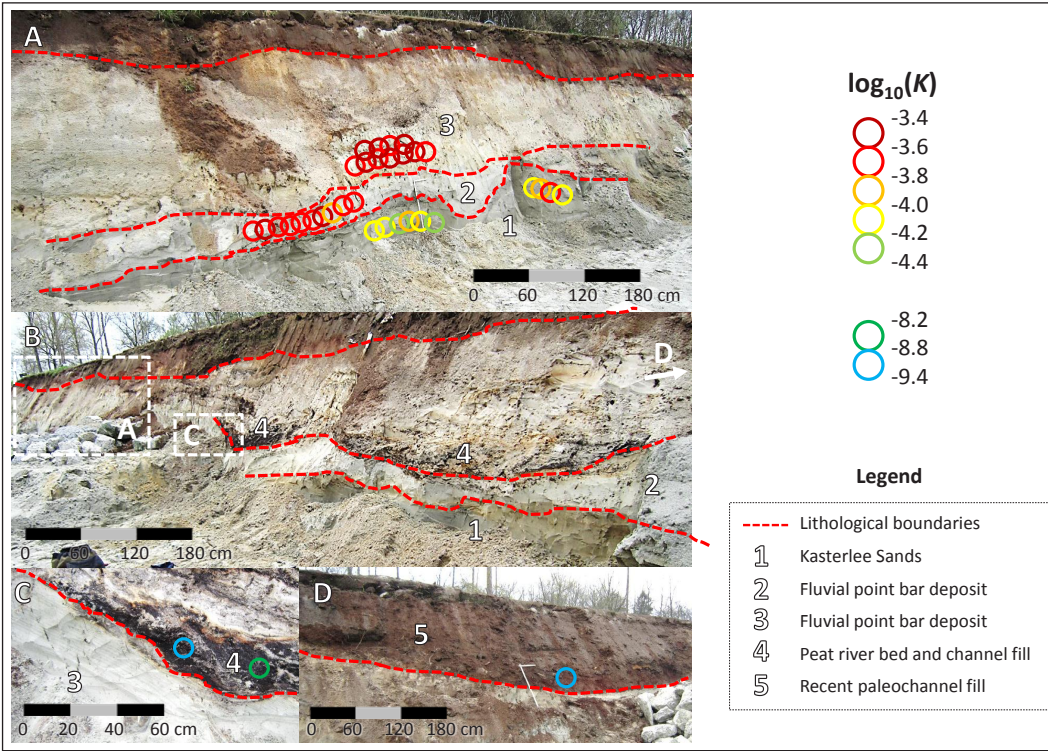
Figure 7. Kleine Nete paleochannel outcrop, with several fluvial point bar sand deposits (A, B), an old paleochannel (C), and the more recent remains (1950s-1970s) of a backfilled meander (D). Positions of the measurements are approximate, as quantification of the contrast between the different units was the main target here.

regular grid was investigated there, and outcrop b and i are not included in the horizontal variography due to the limited horizontal extent of the investigations. Directional experimental variograms for the horizontal (parallel to stratifications) and vertical (orthogonal to stratifications) directions are presented in Fig. 6.

3.1. Quaternary sediments

The Quaternary stratigraphy of Belgium is essentially made up of continental facies deposited by fluvial, eolian, slope or organo-chemical processes (Gullentops et al., 2001). The sediments studied in this paper are estuarine to fluvial, exhibit fine-grained clayey to sandy textures, and belong to the Weelde or Sterksem

Formations, or represent alluvial deposits by the Kleine Nete river.

3.1.1. The Schelde Group

The Schelde Group includes all fluvial deposits in the Schelde and Yser basins. The oldest one corresponds to terraces formed during valley incision in Lower and Middle Pleistocene. Younger deposits are present in the valley bottom fill. Deposits occurring as far upstream as the Kleine Nete basin probably originate from Late Glacial to Holocene filling of Late Glacial incisions (Beerten, 2010).

    Outcrop a: Kleine Nete deposits at Kasterlee

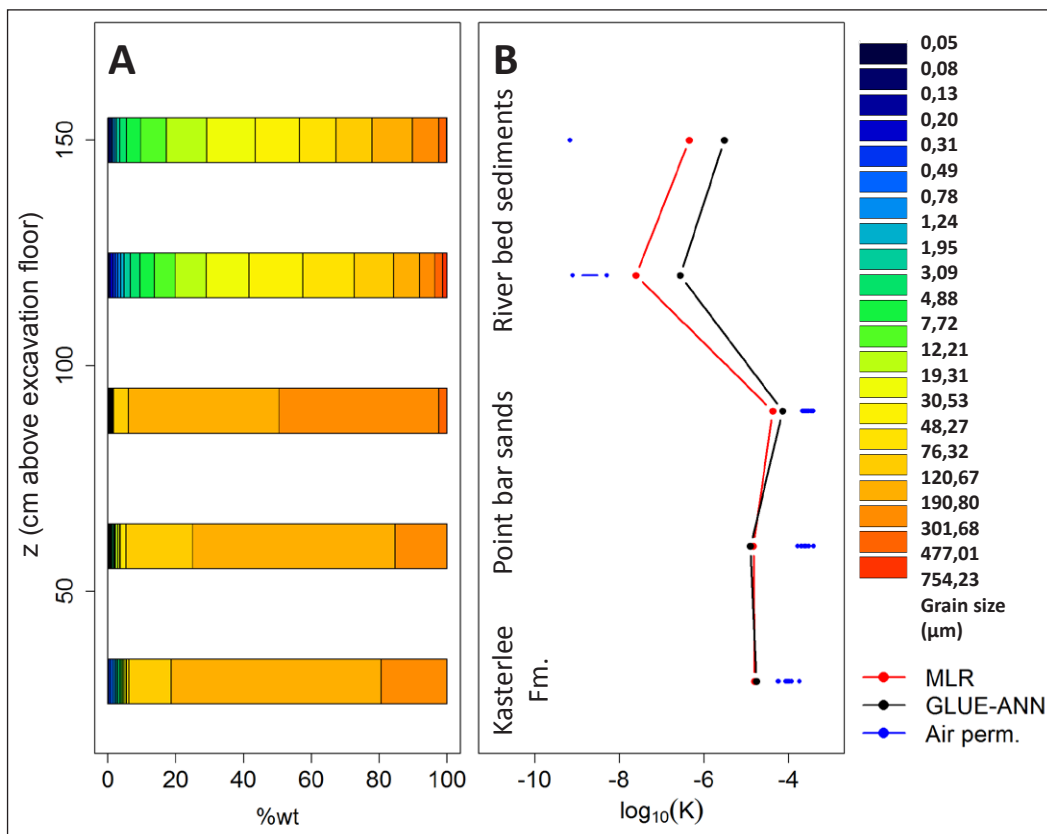Paleo-channels of the Kleine Nete river deposits together with

Figure 8. Grain size distributions (A) and hydraulic conductivities (B) derived from the air permeameter measurements (Air perm.) on the same units, and predicted with the multiple linear regression model (MLR) and GLUE-ANN ensemble of Rogiers et al. (2012) for the Kleine Nete deposits outcrop. The vertical position is approximate, as not all samples were taken at the same position. The soil surface is approximately 2.5 m above the excavation floor.

fluvial point bar deposits were investigated near the city of Kasterlee. Fluvial point bar sands (Fig. 7A,B), a peat paleobedding (Fig. 7C) and a more recent channel fill (Fig. 7D) that finds its origin in the straightening of the Kleine Nete river from the 1950s to the 1970s (De Bie et al., 2007; AMINAL, 2003) are clearly distinguishable. Grain size analysis (Fig. 8) shows point bar sand deposits have more than 95% sand and less than 1% clay. The percentage of fines increases to a few percentages in the lowermost sand unit, which corresponds probably to the Tertiary Kasterlee sands. The peaty river bed and the red-coloured material in the recent channel fill (Fig. 7C, D, and uppermost two samples in Fig. 8) show a few percentages of clay and almost 60% of silt.

Air permeability-derived K values agree reasonably well with predictions based on particle size data; details about the multiple linear regression predictive model (MLR) and the generalized likelihood uncertainty estimation - artificial neural network model (GLUE-ANN) are available in Rogiers et al. (2012). The largest difference between measured and predicted K is for the top of the river bed sediment (Fig. 8). A high moisture content at that and the next depth likely influenced air permeability measurements resulting in low K values. For the point bar sands, this offset seems to be no more than approximately one order of magnitude. Such discrepancies were also reported by Rogiers et al. (2013b) with regards to a comparison between outcrop and subsurface values; the main reason being that the grain size based K-prediction model was developed using subsurface sediments exhibiting slightly different grain size properties than the outcrops. Gridded measurements were not performed on this outcrop, hence no spatial analysis was carried out.

The point bar sands proved to be very homogeneous, as all K values from the air permeameter measurements are within one order of magnitude (Fig. 8). A mean K value of $10^{-3.7}$ m/s indicates very permeable sands (Table 2), hence current surface water bodies that are eroding such sands might show a high degree of connectivity to the groundwater. In contrast, both the channel fill and peat bedding display relatively low K values ($10^{-8.9}$ m/s; such

low values are influenced by the high moisture content (saturation degree > 80%) in these materials; based on a comparison with independent K measurements, the grain size-based predictions are more accurate; see also Rogiers et al. 2013a). Regions where these deposits exist in the river bed are likely to have a low degree connectivity with the groundwater. As the measurements at this outcrop were exploratory, and not performed on a regular grid, this outcrop is not included in the upscaling approach.

3.1.2. The Weelde Formation

The Weelde Formation is part of the Campine Complex (also known as the Kempen Group), and consists of fine grained sandy to clayey sediments, all of which are the result of alternating estuarine and fluvial-eolian conditions at the moment of deposition (Gullentops et al., 2001).

Outcrop b: Weelde Formation at Beerse

The Weelde Formation is accessible through several brickworks quarries at the interfluves between the Nete and Meuse basins in the northern part of the study area. The top 5.5 m of the formation was studied at the Beerse clay pit because the lithological succession could serve as analogue for engineered earth covers whose design is being optimized (Jacques et al. 2010). The 5.5-m deep vertical profile starts at the bottom in the top of a clay layer and is cross-cutting a second clay layer, as shown in Fig. 9.

Grain size analyses for this profile (Fig. 10) reveal the clay percentage ranges from 6 to 18% in the clayey layers, with a pronounced silt content for the central layer (up to 65%). A thin layer of coarse sands (at 40 and 180 cm) is present on top of each of the clay layers, which creates a large difference in lithology on vertical distances of only a few centimetres.

The air permeability-based K values (Fig. 10) clearly show the presence of the central clay layer between approximately 1.6 and 2.6 m. Only a few measurements were performed in the clay itself because of the long equilibration time required to obtain a reliable value; the minimum value measured was $10^{-8.1}$ m/s (Table 2). This low value was used to fill in missing values at
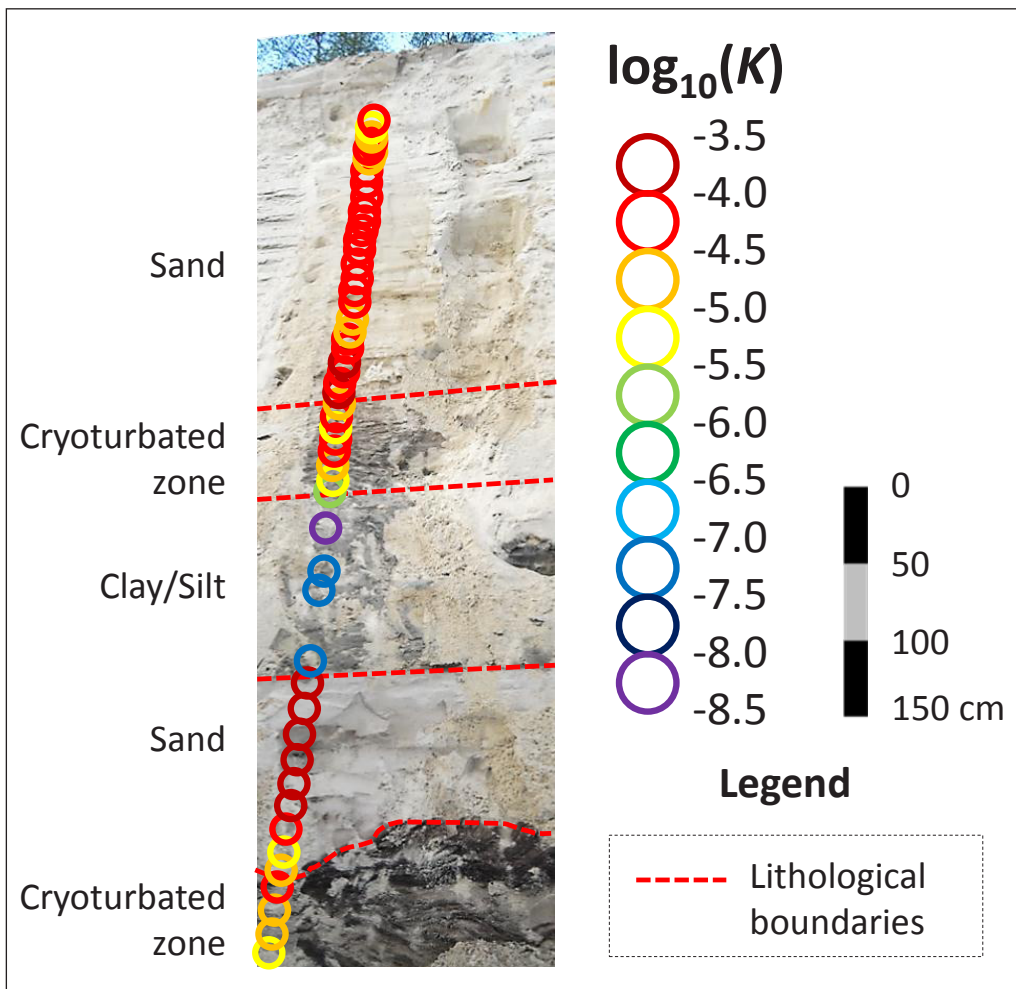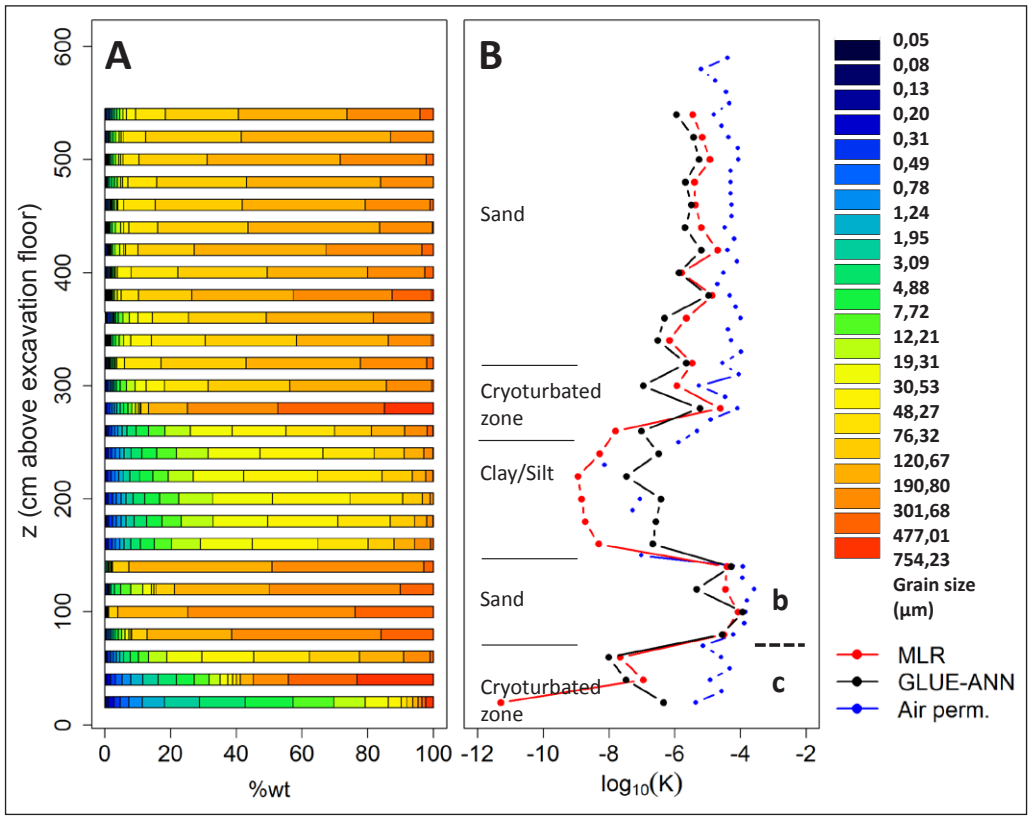

Figure 9.
Campine Complex outcrop.

Figure 10. Grain size distributions (A) and hydraulic conductivities (B) derived from the air permeameter measurements (Air perm.), and predicted with the multiple linear regression model (MLR) and GLUE-ANN ensemble of Rogiers et al. (2012) for the vertical profiles through the Campine Complex outcrop.

several measurement depths within the clay layer on the 10 cm-spaced profile thus facilitating the upscaling later on (Fig. 4b). The grain size based *K* predictions show a similar pattern, but with an offset of about one order of magnitude towards lower values. As indicated above, this offset corresponds to the outcrop – subsurface sediments bias observed by Rogiers et al. (2013b), probably caused by mineralogical weathering processes, physical degradation at the macroscopic scale (i.e. entire clay lenses), differential compaction histories, all of which are not identifiable on the basis of by grain size. The grain size based predictions are not consistent for the samples with a very large silt fraction, since these were not encountered in the borehole data from which the models were derived (see Rogiers et al., 2012). It is worth noting that the extrapolation to these silty grain size distributions by the linear MLR model is more trustworthy than the non-linear extrapolation of the GLUE-ANN model. In terms of spatial correlation structure, the vertical experimental variogram shows clearly the influence of the presence of a clay layer in the central part of the profile (Fig. 6, outcrop b). The small-range variability is comparable to that of the other sandy outcrops studied. The entire vertical profile is used to calculate outcrop-scale parameter values in section 4.

Outcrop c: Cryoturbation and ice wedges in the Weelde Formation, Beerse

A more detailed investigation of the bottom layers of the Campine Complex outcrop (lowest cryoturbated zone in Fig. 10) identified cryoturbation and ice wedges that have disturbed the otherwise sharply delineated clay layer (Fig. 11). The study of such features is relevant since it will alter the hydraulic properties of the clay layer, and quantification of such impacts provides useful underpinning of studies of long-term performance of engineered clay barriers.

This part of the outcrop with its characteristic frost structures exhibits a larger variability in *K* than the measurements in the sediment succession above (Fig. 5, outcrop c versus b). The past mixing of sediments owing to these paleo frost processes will have contributed to this variability with a data range of over five orders of magnitude (Table 2), both in horizontal and vertical direction. Due to cryoturbation and formation of ice wedges and their infillings the spatial rearrangement of the original stratification has been disturbed; as a result this outcrop shows the highest semivariance in horizontal direction for all lag distances (Fig. 6, outcrop c). Several measurements in the clay are missing due to excessively long equilibration times. Therefore the minimum observed value is used to complete the 10-cm spaced grid for the purpose of the upscaling calculations in section 4 (shown in Fig. 4, outcrop c).
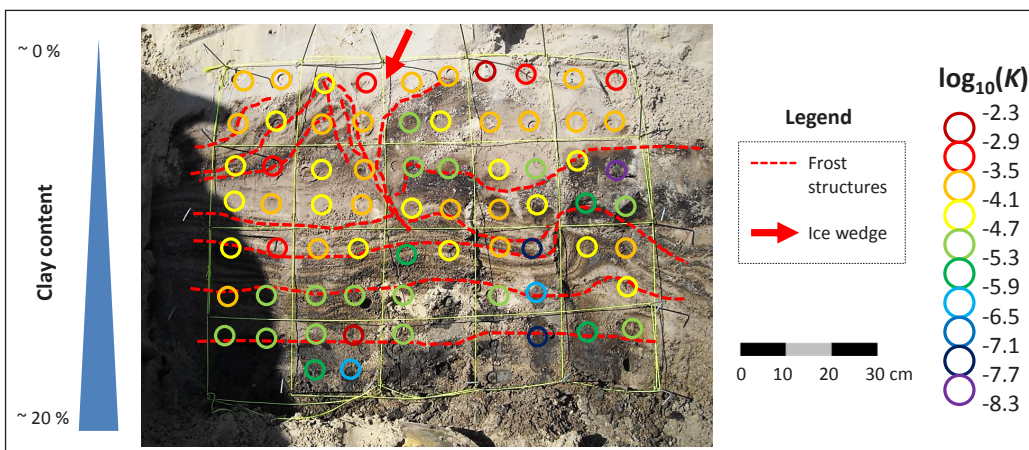

Figure 11. Cryoturbation and ice wedge in the top of a clay layer in the Weelde Formation outcrop. This clay layer appears at the bottom of the profile shown in Fig. 9 with sample locations shown as open circles.

Figure 12. Lommel Sands outcrop showing the Quaternary-Tertiary boundary; also visible are the top of the Mol Formation represented by layers of Mol sand and lignite. The upper six rows of measurements were used for the calculations.
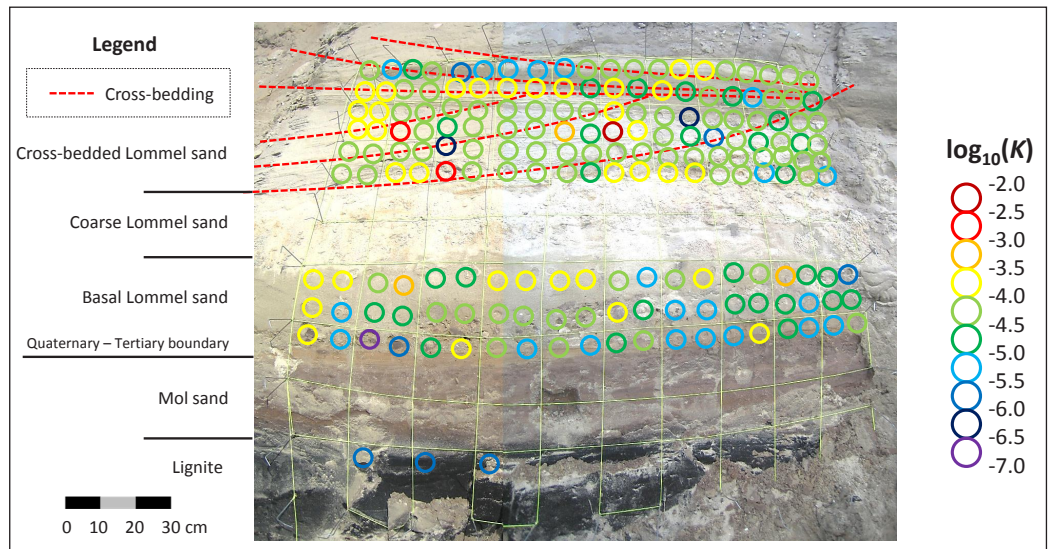
3.1.3. The Sterksel Formation

Coarse gravelly sands were deposited by the Rhine as a braided river (Beerten, 2006), attracted into the Roer Valley Graben by its renewed sinking (Gullentops et al., 2001). The Sterksel Formation occurs in the lower Meuse valley, and is of Early Pleistocene age. The Lommel Member, that covers the Western part of the Kempen, was attracted by the antithetic down warping along the Rauw Fault.

Outcrop d: Lommel Sands at Lommel Maatheide

The Lommel Sands were studied at the Maatheide quarry of Sibelco. They are part of the unsaturated zone through which groundwater recharge takes place; the water table is about 20 cm below the bottom of the outcrop. The thickness of Lommel Sands is up to several meters in the east of the study area (Gullentops & Wouters, 1996). Cross-lamination stratification and fluviatile gully structures are clearly visible on Fig. 12. Within the underlying Mol Sands, a compact lignite layer is present that represents an important hydraulic barrier.

Air permeability measurements were performed with a spacing of 10 cm on a 2 by 1.8 m grid. This resolution might be insufficient to investigate the fine-scale layering within the cross-bedded fluviatile gullies (about half a meter high and a few meters wide), but a clear contrast exists at the boundaries between gullies, which is also indicated by the visual colour contrasts and the air permeameter measurements (Fig. 12). Hydraulic conductivity clearly varies over several orders of magnitude within the Lommel Sands, even within one single gully (Table 2; Fig. 5). There are missing K values at two depths: the sandy material at the middle

part of the outcrop was too coarse and loose for making reliable measurements; furthermore, the bottom part was too wet owing to the shallow groundwater table. Three measurements could however be performed within the lignite layer, with an average of $10^{-5.8}$ m/s (not shown). This indicates that these 0.5- to 1-m thick compacted banks function as important hydraulic barriers within the Mol Sands. The spatial variability seems to be more or less equal in horizontal and vertical directions, and there is little spatial structure over the short distances investigated (Fig. 6, outcrop d). Further upscaling analyses are done in section 4 on the upper 60 cm of the measurement grid within the Lommel Sands (Fig. 4d), because several measurements are missing at depths greater than 60 cm below the top of the grid, and the lignite is considered to be a quite homogeneous unit. One single missing value was interpolated from its neighbours to complete the grid.

3.2. Pliocene sediments

3.2.1. The Mol Formation

The Tertiary Mol Formation consists of white, pure (99% SiO_2) (Sibelco, 2010), coarse and medium fine continental/estuarine sands, sometimes lignitic and with some lenses of micaceous clay (Laga et al., 2001). The bottom part is very slightly glauconiferous (less than 2 %) (Beerten et al., 2010). Within the geographic boundaries of the Mol municipality, the 20–m thick Mol Formation is divided into the Upper Mol and Lower Mol Sands, both Pliocene in age (Beerten et al., 2010). The latter are very well sorted and finer and darker in colour, while the former
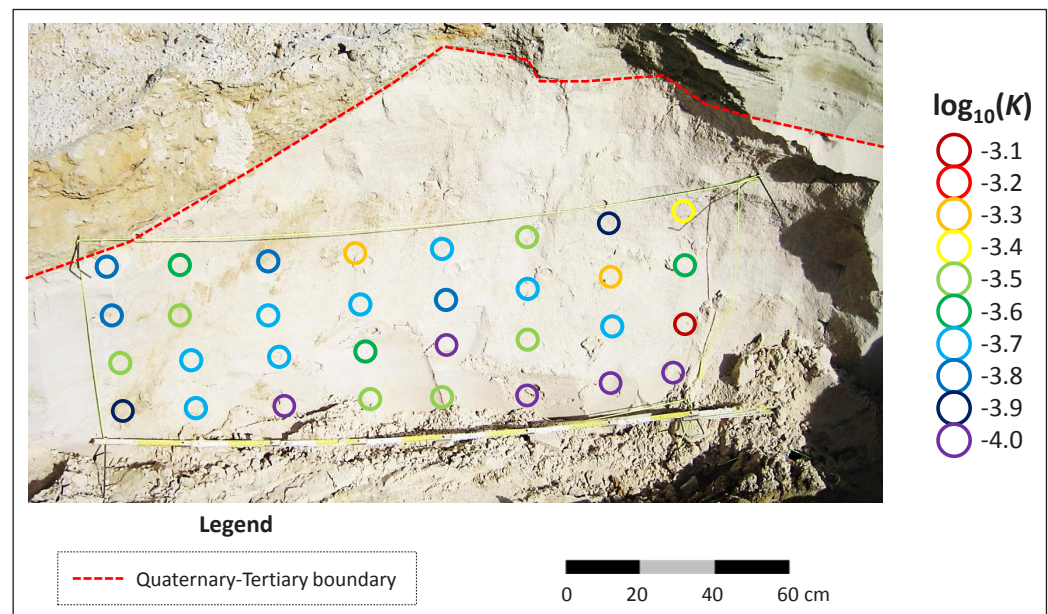

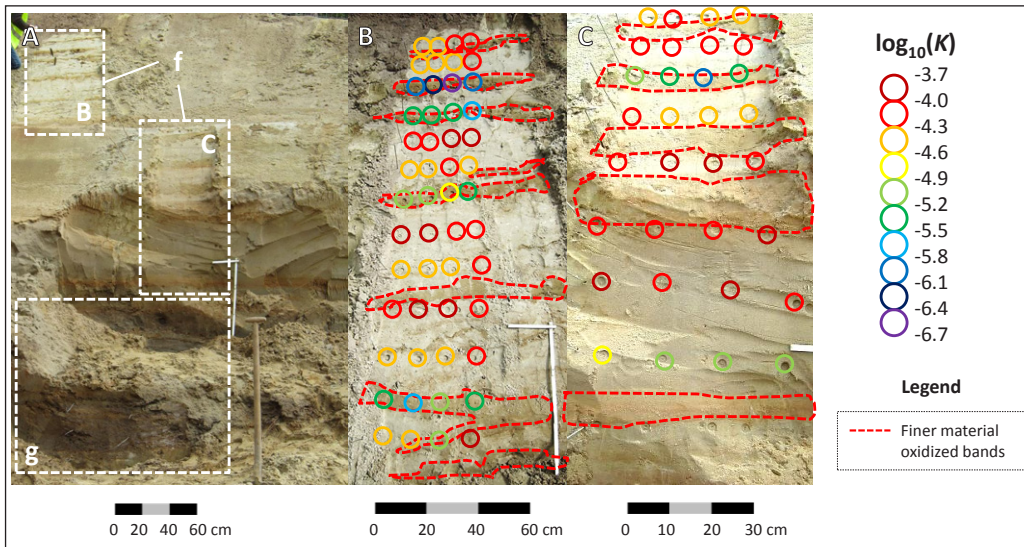**Figure 13.** Mol Sands outcrop showing the Quaternary-Tertiary boundary.

Figure 14. Overview (A) of three sampling zones; top part of the Poederlee Sands outcrop at Kasterlee with distinct fine-grained oxidized bands (B, C), denoted as outcrop f.
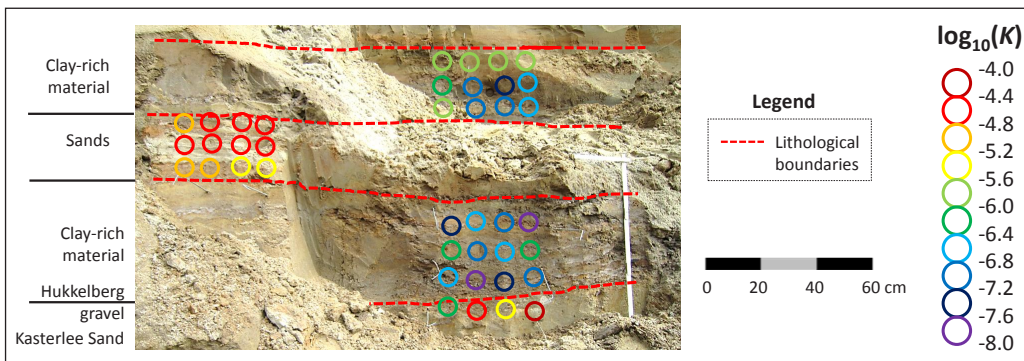

Figure 15. Bottom of the Poederlee Formation at Kasterlee with several pronounced clay lenses; the Hukkelberg basal gravel indicates the boundary with the Kasterlee Sands.
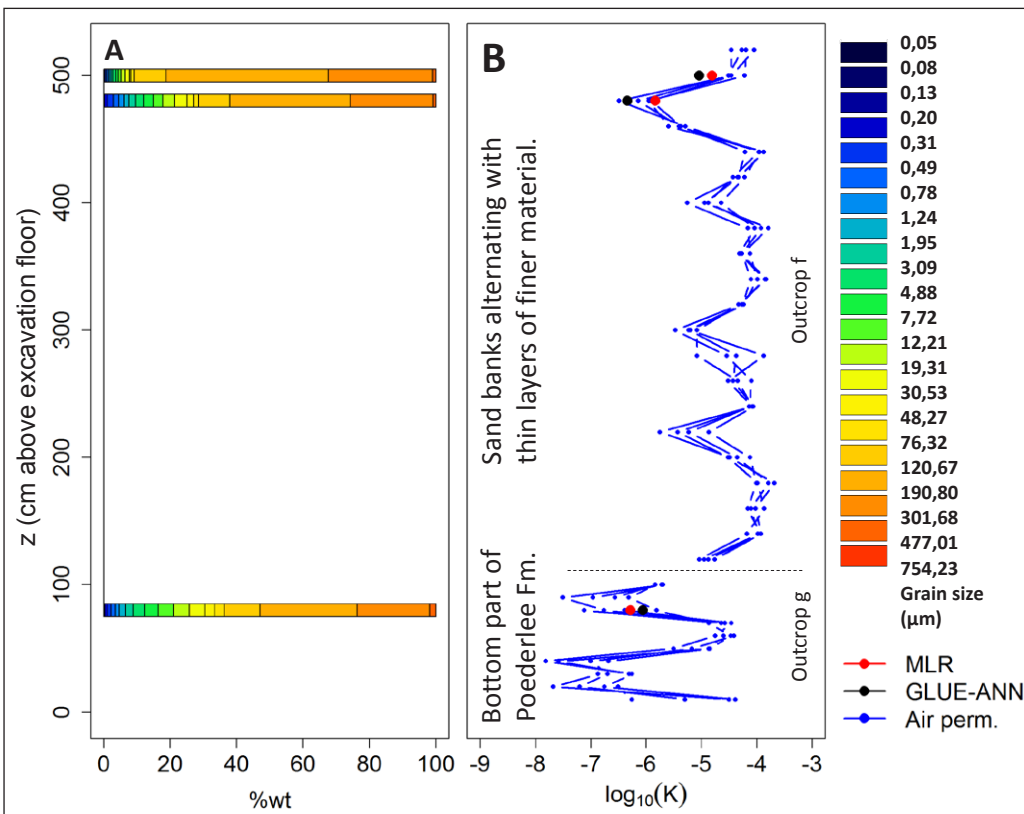

Figure 16. Grain size distributions (A) and hydraulic conductivities (B) derived from the air permeameter measurements (Air perm.), and predicted with the multiple linear regression model (MLR) and GLUE-ANN ensemble of Rogiers et al. (2012) for the Poederlee outcrop at Kasterlee. The connected dots represent vertical transects.

are moderately to well sorted medium sands with a basal gravel layer. Because of the high siliceous content of this sand, it is being mined for various industrial uses (Gullentops and Wouters, 1996). One outcrop site was investigated at the municipality of Lommel.

Outcrop e: Mol Sands at Lommel

These Pliocene sands occur one to two meters below the water level of the dredging pond at the Maatheide quarry, but the depth of the Quaternary-Tertiary boundary shows considerable variation. A clear boundary was observed just below the ground surface, and a small outcrop was excavated, as shown in Fig. 13. Except for some small oxidized horizontal bands, no sedimentary structures could be distinguished in these Mol Sands.

Because the material is very loosely packed, a sampling density of 20 cm spacing was applied to prevent collapse of the excavation. The average K value amounts to $10^{-3.7}$ m/s, which

indicates a very permeable material (Table 2). Spatial correlation is hard to detect (Fig. 6, outcrop e), but the variability within this outcrop clearly is very small with all K values within a range of less than one order of magnitude The difference between these K values and those of the underlying lignite layer (see Lommel Sands outcrop) again underlines the role as hydraulic barrier of the latter ($10^{-3.7}$ versus $10^{-5.8}$ m/s). These continental/estuarine sands seem to compare very well in hydraulic characteristics sense with the Kleine Nete point bar deposits, with a very similar CV (Table 2, Fig. 5, outcrop a and e) and only slightly visible sedimentary structures (e.g. point bars left of the peat in Fig. 7C). The difference with the fluviatile Lommel Sands ($10^{-3.7}$ for Mol Sands versus $10^{-4.21}$ m/s for Lommel Sands) is probably due to the different grain size characteristics (Lommel being more heterogeneous and less well sorted than Mol) and depositional conditions (fluviatile versus estuarine). The entire measurement grid is used for upscaling calculations in section 4, as shown in Fig. 4.

3.2.2. The Poederlee Formation

The Poederlee Sands are fine, slightly glauconiferous sands, with small lenses of clay in the lower part (Laga et al., 2001). They are lateral equivalents of the Mol Sands (Vandenberghe et al., 2004; Louwye & De Schepper, 2010). The oldest depositional environment of the Poederlee Formation was neritic with an open ocean influence, later changing into more shallow waters in the proximity of the coast with fresh water influence (Louwye & De Schepper, 2010). Deposition likely took place during a transgressive to highstand phase, under a high and possibly maximal sea level, until the accommodation space was filled. The Poederlee Sands were studied at two locations, i.e. Kasterlee (Figs 14-16) and Lichtaart (Fig. 17).

Poederlee Sands at Kasterlee were analysed in two parts: an upper part (denoted further on as outcrop f) includes two sampling zones (Figs 14A, B & C) and the lower part (denoted further on as outcrop g) encompasses one sampling zone (Figs 14A & 15).

Outcrop f: Poederlee Sands at Kasterlee (top of outcrop)
This upper part of the Poederlee Formation exhibits several bands of fine oxidized material within a background of white fine sand, with sand contents of respectively 70 and 90% (Figs 14B, C & 16).
This part of the Poederlee Sands at Kasterlee shows a mean K value of $10^{-4.5}$ m/s with a standard deviation of 0.61 (Table 2). The measurements were done with 20 cm spacing in vertical direction and 10 to 15 cm in horizontal direction. The variability expressed in terms of a three orders of magnitude range is caused by the presence of the horizontal bands composed of finer-textured material within the more permeable sand; lower K values typical of the finer-textured bands are clearly visible in Figs 4 (outcrop f) and 14. As a result the horizontal spatial variability is considerably

smaller than the vertical one (sill for horizontal variogram is ~0.05 versus ~0.4 for the vertical) (Fig. 6). All measurements in Fig. 14B & C are combined (see Fig. 4) and used to calculate outcrop-scale parameter values in section 4.

Outcrop g: Poederlee Sands at Kasterlee (bottom of outcrop)
The bottom part of the Poederlee Sands outcrop at Kasterlee (Figs 14 & 15) exhibited layers with increased clay and silt content (resp. 6 and 30%), ranging in thickness from a few centimetres to several tens of centimetres. Presence of the basal Hukkelberg gravel (Laga et al. 2001) indicated that these sediments correspond to the bottom of the Poederlee Formation.

The average K value for outcrop g is $10^{-5.94}$ m/s, and the standard deviation (1.07) is one of the highest observed (Table 2). Also worth noting is that the maximum value is the lowest maximum observed across all outcrops (Fig. 5).

The few hydraulic conductivities predicted from the grain size analyses of outcrops f and g confirm the air permeameter-derived values (Fig. 16). Although only three grain size predicted K values exist, it is useful to discuss the absence of an offset which was observed for other outcrops. A reason for this might be the fact that the outcrop was only very recently excavated for a tunnel project, and there are still a few meters of overburden above the highest measurement point. As a consequence, the sediments have not been influenced by weathering processes, physical degradation of sediment structure, migration of clay particles, root penetration, etc. For a comparison between outcrop-derived and hard subsurface data, the reader is referred to Rogiers et al. 2013b. At Kasterlee, the basal part of the Poederlee Formation thus represents potentially a very important hydraulic barrier. The horizontal spatial variability seems to be moderate (sill ~0.2), while the vertical variability seems to be very high at short ranges (sill ~1-2) (Fig. 6). As the main heterogeneity occurs in the vertical direction, all measurements are combined into a 10-cm spaced grid, as shown in Fig. 4, for the upscaling calculations in section 4.

Outcrop h: Poederlee Sands at Lichtaart
At the Poederlee Sands outcrop in Lichtaart we observed oxidized horizons several cm-thick in addition to extensive bioturbation features and the Hukkelberg base gravel (Fig. 17). Sedimentary structures such as small-scale foresets and bottomsets were not distinguishable. The clay content increases towards the bottom of the formation, in the form of a few distinct small clay lenses.

While the Poederlee Sands outcrops at Kasterlee (Fig. 15) and Lichtaart (Fig. 17) are about 2.5 km apart, there is a noticeable difference in the geometry of the clay lenses in the bottom of the Poederlee Formation. In Kasterlee the clay lenses are fewer in number and are up to tens of centimetres thick, while in Lichtaart there are many lenses of less than a centimetre thick.

A clear vertical trend is visible in the K matrix of the outcrop (see Fig. 4), which was measured with a 10 cm spacing. This
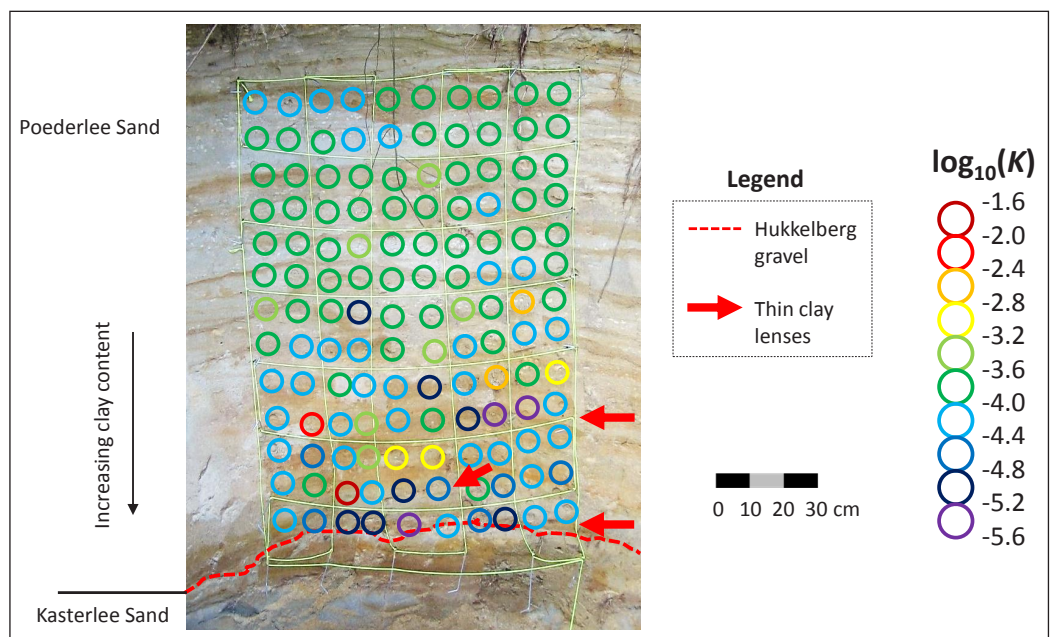

Figure 17. Bottom of the Poederlee Formation at Lichtaart, including a few very thin clay lenses (see arrows), and the Hukkelberg basal gravel.
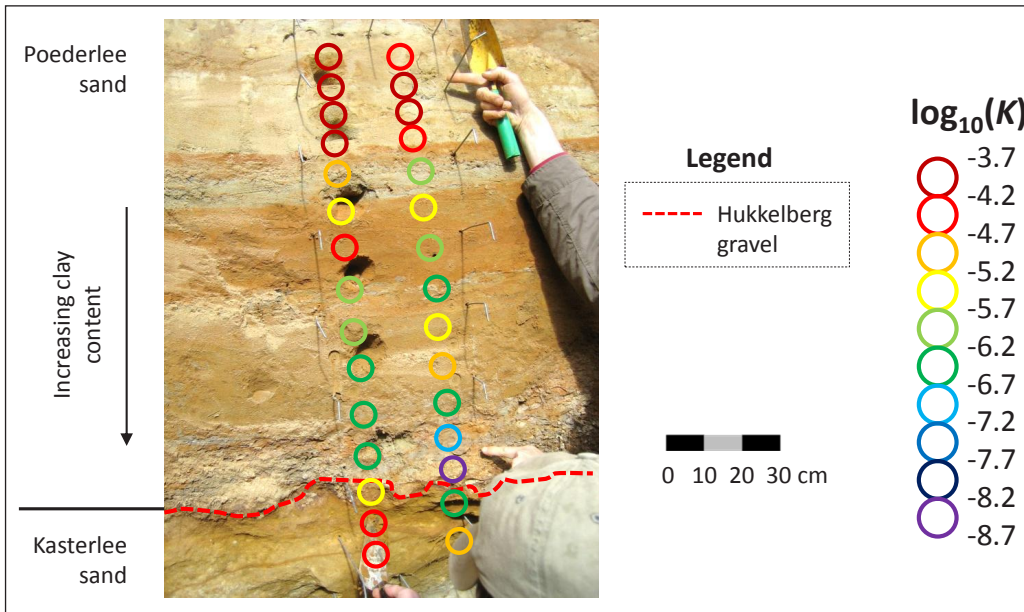
Figure 18. Transition between the Poederlee and Kasterlee Sands at Lichtaart including the Hukkelberg gravel stratigraphic boundary.
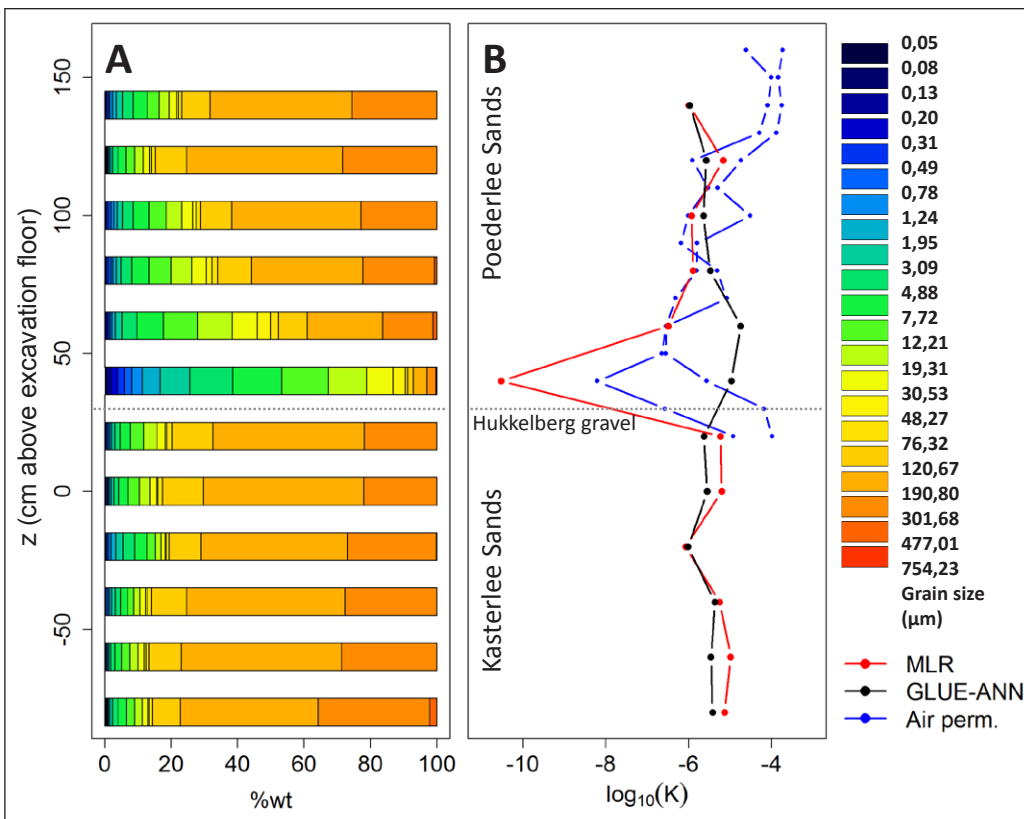

Figure 19. Grain size distributions (A) and hydraulic conductivities (B) derived from the air permeameter measurements (Air perm.), and predicted with the multiple linear regression model (MLR) and GLUE-ANN ensemble of Rogiers et al. (2012) for the Poederlee-Kasterlee transition.

reflects the increasing clay content and heterogeneity towards the base of the Poederlee Sands at this site. The volume occupied by clay lenses is however very different from that at the bottom of the formation at Kasterlee. A significant correlation between K values and the brown-coloured oxidized horizons could not be observed, although at some levels the conductivity is slightly lower in such horizons. The overall mean K value is $10^{-3.9}$ m/s, with a relatively small $log_{10}(K)$ variance of 0.28 (Table 2). The $log_{10}(K)$ range however goes up to 3.88 due to the trend in the bottom of the outcrop. The horizontal direction exhibits spatial structure and the vertical short-range variability is rather high (Fig. 6, outcrop h). The entire measurement grid is used to calculate outcrop-scale parameter values in section 4.

Outcrop i: Poederlee-Kasterlee transition zone, Lichtaart
The Hukkelberg gravel is the compact basal gravel bed of the Poederlee Sands and forms the transition towards the underlying Kasterlee Sands (Fig. 18). It consists of rounded quartz and flint pebbles and silicified carbonates (Laga et al., 2001). Above this layer, the clay content again clearly shows elevated values

in the bottom of the Poederlee Formation (Fig. 19). The gravel layer itself is compacted and cemented and includes several concretions up to several centimetres in size. Such a layer increases the anisotropic nature of the hydraulic conductivity tensor and thus has implications for the water flow across this stratigraphical boundary. Currently the concretions occur in the unsaturated zone; however several borehole cores from aquifer sediments (Beerten et al. 2010) also contained similar concretions indicating such structures might have formed at different times during the Poederlee-Kasterlee and Kasterlee-Diest hiati in palaeo-unsaturated conditions.

The air permeameter measurements were performed across the stratigraphical boundary on two profiles 30 cm apart using a vertical spacing of 10 cm. The bottom of the Poederlee sands shows an increasing clay content towards the compacted and cemented gravel layer and hence displays lower K values (Figs 4, 18 & 19). This outcrop has a mean K value of $10^{-5.28}$ m/s and the highest variance of K (1.29 see Table 2), which can be attributed to grain size variations (lower K due to increasing clay content),

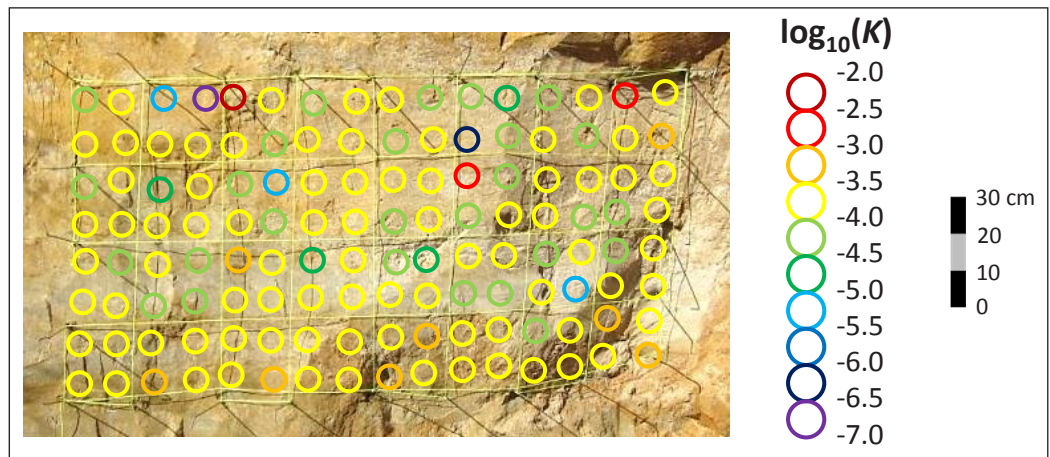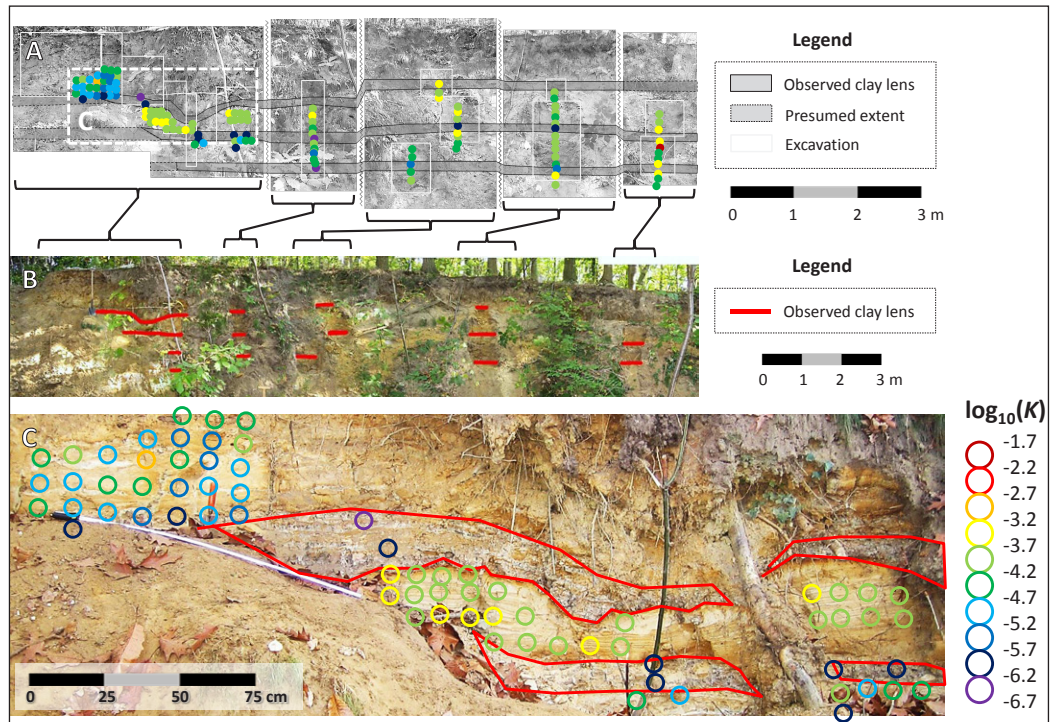**Figure 20.** Stuctureless Kasterlee Sands outcrop.

Figure 21. Kasterlee Clay outcrop at Heist-op-den-berg. A: Excavated profiles with clay lens connectivity. B: Overview of the entire outcrop with observed clay lenses. C: Detail of clay lenses with root penetration causing weathering of the clay.

post-depositional oxidation (lower *K* with increasing oxidation features) and cementation processes yielding lower *K*. The Hukkelberg gravel bed is very thin and not always continuous. Hence it is not likely to influence the hydraulic properties across this profile. The vertical variability increases with distance until about 1 m (Fig. 6B). All measurements displayed in Fig. 18 are used to calculate outcrop-scale parameter values in section 4.

The grain size analyses of this section of the profile are presented in Fig. 19. The samples are taken more or less each 20 cm. The increasing amount of silt and clay content towards the base of the Poederlee Sands is very clear. Below the base, the sand content increases to more than 80% in the Kasterlee unit. The Hukkelberg gravel itself was not sampled since it was very thin, and probably contains too much coarse fragments for grain size analysis using the laser diffractometer. Note that all grain size distributions are bimodal in this profile, with virtually no particles between 30 and 50 μm. The grain size based hydraulic conductivity predictions correspond reasonably well with the air permeameter based values. Only the sample at the base of the Poederlee Formation, exhibiting a very high fine silt content, seems to have lower conductivities based on the MLR grain size model. This clearly shows that physical degradation of the sediment structure has a larger effect on the clayey parts of the studied outcrops than the fraction of sand particles. The GLUE-ANN model fails to make correct predictions since such high fine silt fractions were not present in the borehole data used to generate (i.e. train) the model (Rogiers et al. 2012).

3.3. Miocene sediments

3.3.1. The Kasterlee Formation

The Kasterlee Formation consists of a relatively homogeneous fine, micaceous, slightly glauconitic, sandy upper part (Laga et al., 2001), and a very heterogeneous alternation of clay lenses and sand banks in the lower part (Beerten et al., 2010). The homogeneous upper part is referred to as Kasterlee Sands while the heterogeneous lower part is named Kasterlee Clay. The depositional environment for this formation is coastal or a coastal embayment, with manifest river influence (Louwye et al., 2007).

Outcrop j: Kasterlee Sands at Lichtaart

Based on analysis of hand-augered boreholes several meters deep, the site at Lichtaart shows no presence of the clay lenses within the bottom part of the Kasterlee Formation. This outcrop (Fig. 20) can therefore only be used as an analogue for the Kasterlee Sands. Except for some oxidized horizons, sedimentary structures were difficult to distinguish, suggesting a fairly homogeneous material commensurate with the typical lithological characteristics of Kasterlee Sands.

The Kasterlee Sands show a mean *K* value of $10^{-3.9}$ m/s at the Lichtaart site (Table 2). While the standard deviation is limited (0.5), several outliers are present (Fig. 5), causing a *K* range of over four orders of magnitude. The lack of clear spatial structures or trends is also visible from the pure nuggets in the experimental variograms (Fig. 6). The entire measurement grid is used to calculate outcrop-scale parameter values in section 4.
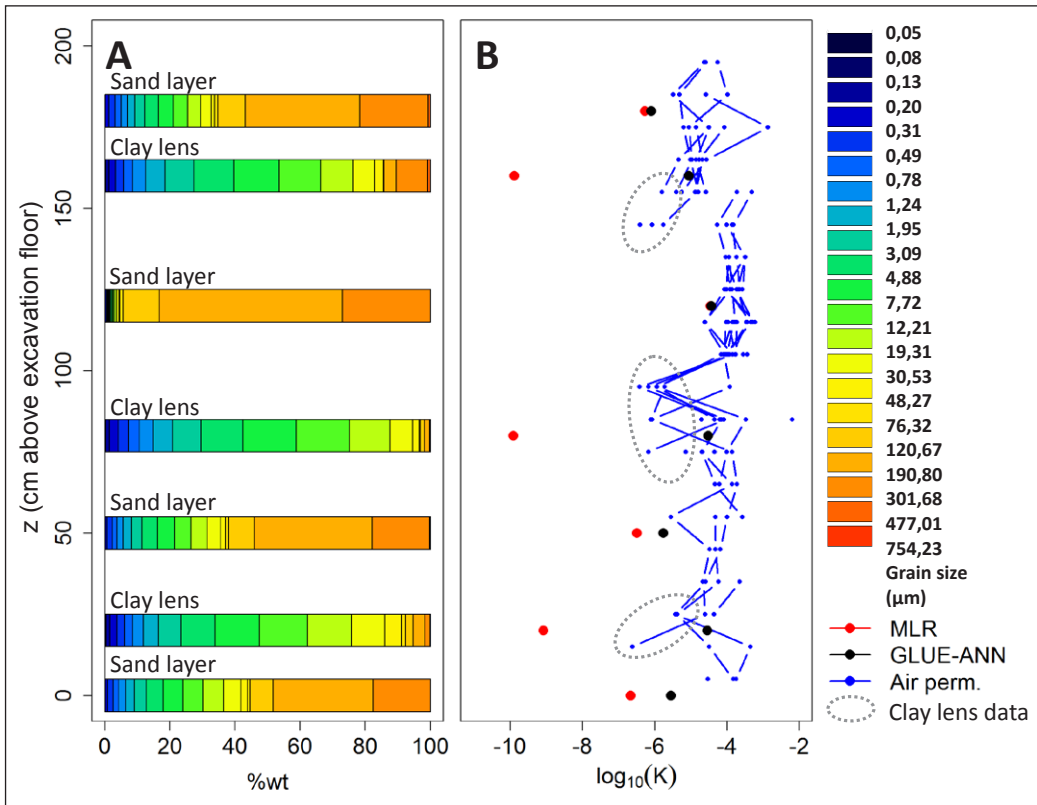
Figure 22. Grain size distributions (A) and hydraulic conductivities (B) derived from the air permeameter measurements (Air perm.), and predictions based on the multiple linear regression model (MLR) and GLUE-ANN ensemble of Rogiers et al. (2012) for the Kasterlee Clay outcrop at Heist-op-den-berg. One grain size sample was taken within each lithological unit. The connected dots represent vertical transects.

Outcrop k: Kasterlee Clay at Heist-op-den-berg

The exposures on the Heist-op-den-berg and Beerzelberg hilltops are useful analogues for the Kasterlee Clay as previous studies identified the presence of the Kasterlee Formation with several thick clay lenses (Fobe, 1995). We studied the sediments in a sunken lane towards the hilltop providing exposure over several tens of meters. Clay lenses were found to be continuous at the scale of the outcrop (about 16 m, Fig. 21A & B). The lenses were heavily affected by physical weathering (e.g., root penetration, frost/thaw cycles; see Fig. 21C). This would possibly cause their hydraulic conductivity to be significantly higher than that of similar unweathered layers, and therefore the outcrop-scale hydraulic conductivity anisotropy would be smaller than that of unweathered layers such as those of the Kasterlee Clay aquitard.

In the left part of the outcrop, measurements were performed each 10 cm, while in the middle and right section, four vertical profiles were sampled. Measurements were performed on the clay lenses and the intercalated sand layers. The lowest K values were observed in the clay, ~ $10^{-6.6}$ m/s (Table 2), which is still relatively high given the high clay content (20%) and low sand content (< 15%; see Fig. 22). This can probably be explained by the fact that the clay is heavily weathered, also resulting in less variability and higher values for the clay than the bottom of the Poederlee Formation (outcrop g) and the transition to the underlying Kasterlee Sands (outcrop i; Fig. 5). Remarkably, the sand banks separated by these clay lenses showed clear differences in K. The upper one shows a clay content of 10% and silt content of 20% (Fig. 22), while K ranges from 10^{-4} to $10^{-5.5}$ m/s. The second sand bank has a sand content of more than 90%, and shows higher hydraulic conductivity values, between 10^{-3} and 10^{-4} m/s. The third sand bank is again similar to the first one, both in terms of hydraulic conductivity and grain size, as is the fourth one. The differences between these sand banks however seem to be less pronounced towards the right part of the outcrop, indicating that the horizontal correlation length within the sand might be at least several meters. The horizontal experimental variogram indeed shows a steady increase in variability with distance, but for the vertical one a pure nugget is present (Fig. 6).

To provide a full matrix of hydraulic conductivity values for the upscaling calculations for the Kasterlee Clay outcrop, a variogram model was fitted to the measurements within the sands only. Next, a geostatistical simulation was performed to fill in the sands, while a constant value was used for the thick clay lenses. This is justified since the weathered state of the clay made it difficult to obtain reliable measurements. Therefore the lowest value was used. The heterogeneity within the sands determines the horizontal K value, and given the limited amount of data, this geostatistical approach has been applied. For more details, the reader is referred to Rogiers et al. (2013a). The results of this simulation are shown in Fig. 4, and represent the entire outcrop section displayed in Fig. 21B. These are also used to derive outcrop-scale parameter values in section 4.

The grain size analyses for the clay lenses and the sand banks in between are shown in Fig. 22. The clay lenses have a clay content up to 20%, more than 70% of silt and only a few percent of sand. The sand banks have less silt (< 45%) and clay (< 10%); different sand banks however have a different particle size distribution. The difference between grain size and air permeameter based hydraulic conductivity values is again very clear. Also for the more sandy material, a consistent offset exists.
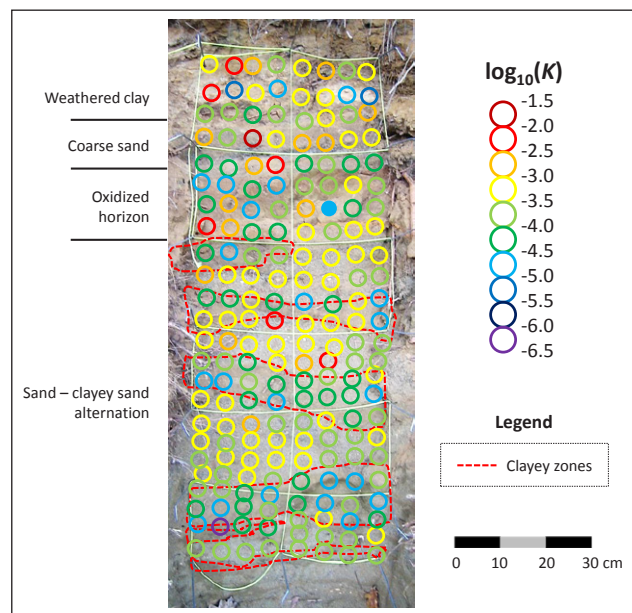

Figure 23. Diest Clayey Top outcrop.

The high fine silt contents again cause the GLUE-ANN model to provide erroneous predictions.

3.3.2. The Diest Formation

The Diest Formation consists of grey green to brownish, mostly coarse, locally clayey, glauconiferous sand, often with sandstone layers (Laga et al., 2001). Glauconite content can be as high as 50 wt% (Beerten et al., 2010). The Diest Sands were deposited as sandbanks migrating over an erosive surface, and were influenced by coast-parallel tidal currents (Wouters & Vandenberghe, 1994). Paleontological evidence suggests that prolonged marginal marine conditions must have prevailed during the Late Miocene (Louwye & Laga, 2008).

Outcrop l: Diest Clayey Top at Heist-op-den-berg

The Heist-op-den-berg outcrop contains only the upper part of the Diest Formation, referred to as Diest Clayey Top by Beerten et al. (2010). This is a relevant analogue layer as it was previously observed in nearly all aquifer boreholes used to develop the hydrogeological model for the Neogene aquifer (Beerten et al., 2010). In all boreholes the Diest Clayey Top was overlain by the Kasterlee Clay. At its bottom, the outcrop consists of an alternation of sands with some darker-coloured clayey zones (Fig. 23). At its top we observed an oxidized horizon containing concretions overlain by coarse sands which in turn were covered by more clayey material. The coarse sands are believed to be a weakly developed basal gravel corresponding to the base of the Kasterlee Formation (Fobe, 1995).

Air permeameter measurements were performed at 5 cm spacing because of the more visually distinguishable heterogeneity. The clayey zones, together with the coarse sand, are clearly the most important features determining hydraulic conductivity heterogeneity. Hydraulic conductivity for the clayey zones ranges between 10^{-4} and 10^{-6} m/s. For the sand in between the clayey zones, values are higher than $10^{-4.5}$ m/s, while the coarse sand shows values higher than $10^{-3.5}$ m/s (Fig. 4). The range is similar to that of the Kasterlee Clay outcrop, but the K values are higher by a factor five (Table 2). Spatial correlation is clearly present in the horizontal direction, but is less apparent in the vertical (Fig. 6, outcrop l). The entire measurement grid is used to calculate outcrop-scale parameter values in section 4.

Grain size analyses performed on the clayey zones and the typical sands (Fig. 24) illustrate a transition from a generally fine to slightly coarser material, with pronounced heterogeneity in the entire profile, as shown by the air permeability K estimates. The systematic offset between the grain size based predictions is again present in the entire outcrop.

Outcrop m: Diest Sands at Lummen

The outcrop of the Diest Sands in Lummen is situated on a remnant hill resisting erosion because of iron sandstones at the top of the sediments. The studied outcrop exhibits typical

Figure 24. Grain size distributions (A) and hydraulic conductivities (B) derived from the air permeameter measurements (Air perm.), and predicted with the multiple linear regression model (MLR) and GLUE-ANN ensemble of Rogiers et al. (2012) for Diest Clayey Top outcrop. The connected dots represent vertical transects.
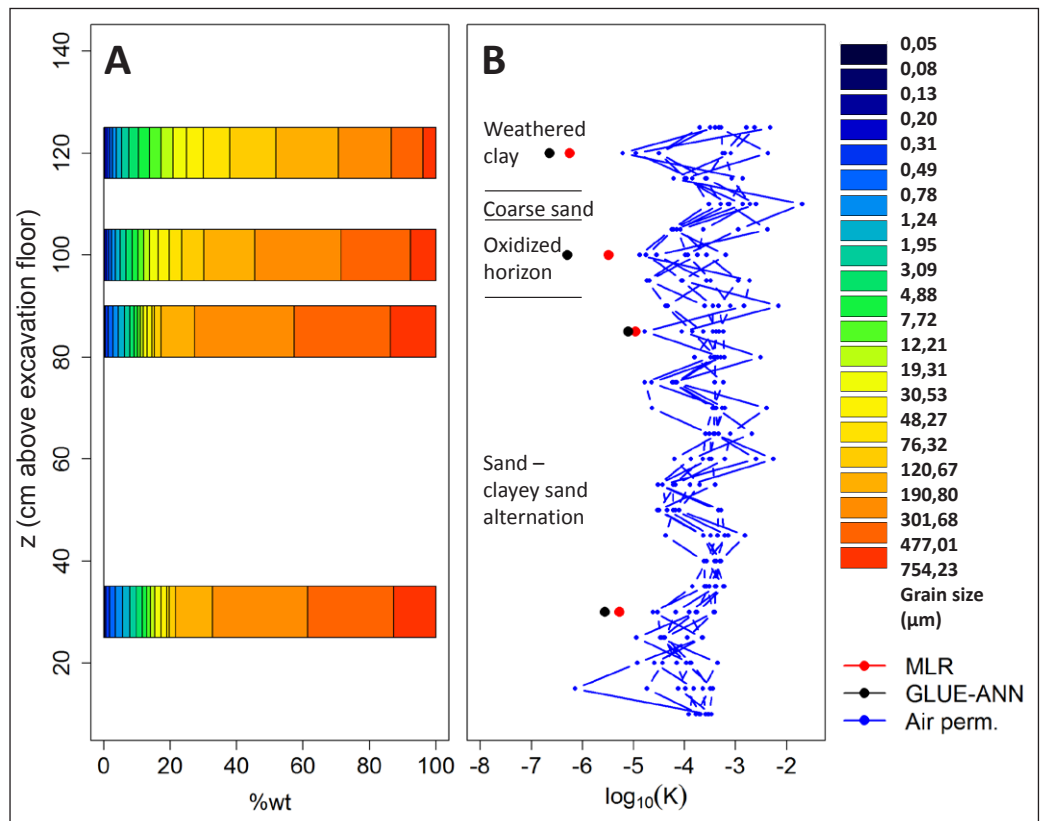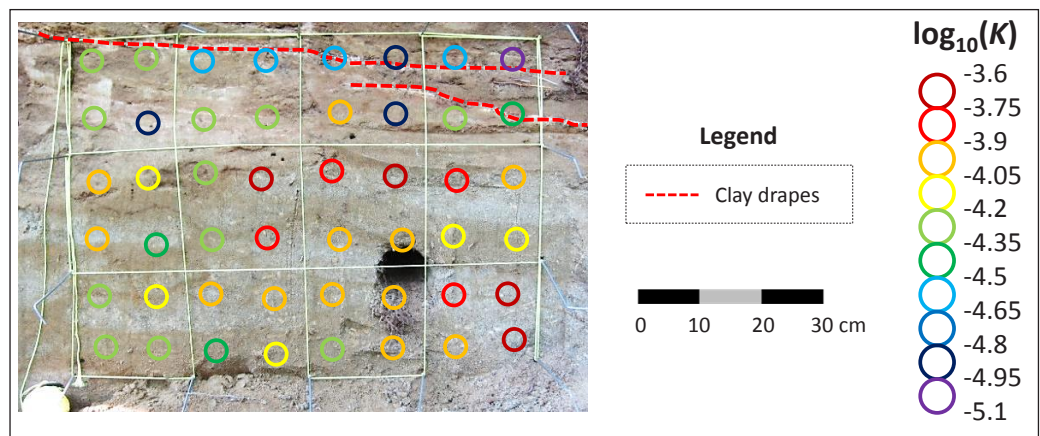

Figure 25. Diest Sands outcrop with thin clay drapes, bioturbations throughout the lower half of the outcrop, and oxidized patches.
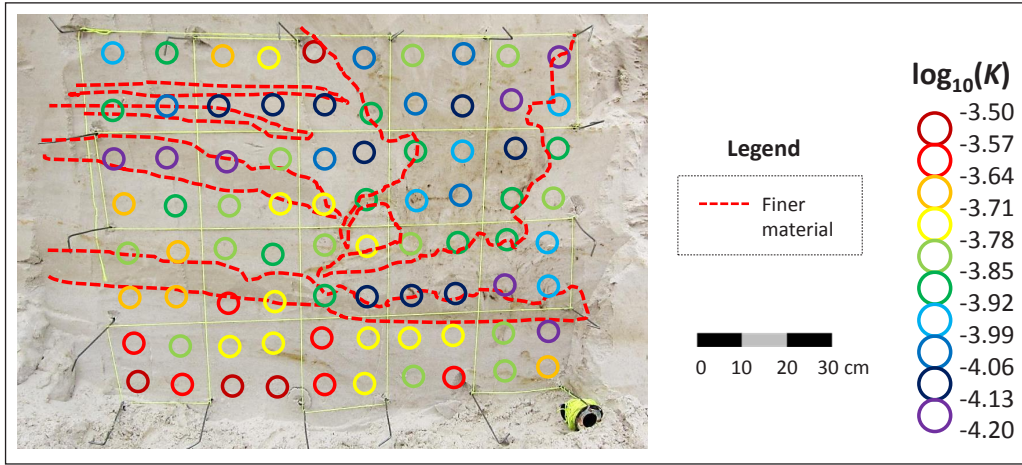
Figure 26. Upper Bolderberg Sands outcrop showing bands of finer material and oxidized patches.

bioturbation structures and high glauconite content and shows several oxidized zones typical of the iron rich sands. A few thin clay lenses or clay drapes are present as well (Fig. 25).

The air permeameter measurements show a mean K value of $10^{-4.1}$ m/s (Table 2). The K range exceeds one order of magnitude, making it more heterogeneous than the Mol Sands, but less than the Poederlee and Kasterlee Sands (Fig. 5). The spatial variability clearly increases with distance, reaching a higher sill level in the vertical (~0.2) than horizontal (~0.08) direction (Fig. 6, outcrop m). The sampling density and the small measurement support did not allow including the very thin clay drapes in the analyses. Due to their limited horizontal continuity, however, they are probably not that important at larger scales. The contrast with the very heterogeneous Diest Clayey Top outcrop is not as expected, and it is doubtful that these outcrops are representative of the respective lithological units. The entire measurement grid is used to calculate outcrop-scale parameter values in section 4.

3.3.3. The Bolderberg Formation

The Bolderberg Formation is a lateral succession of marine to continental sandy deposits (Laga et al., 2001). The white, fairly coarse sands with lignite layers and glassy quartzite banks, referred-to as Genk member, are studied here. Both outcrops (Figs 26 & 27) are located in the Sibelco quarry at Maasmechelen, where several meters of Meuse gravels overlie the Bolderberg Formation.

Outcrop n: Bolderberg Sands at Maasmechelen (upper part) The upper outcrop (Fig. 26) is located only a few meters below
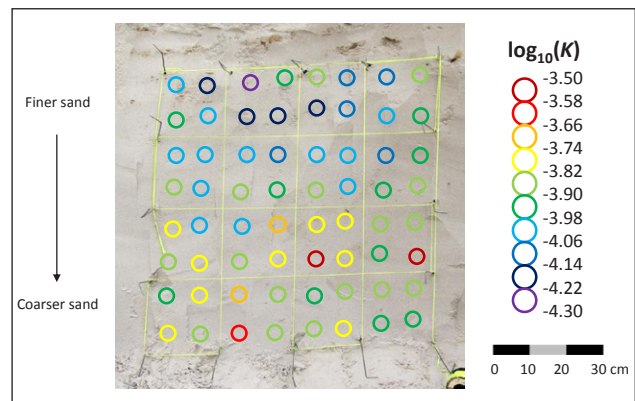

Figure 27. Very homogeneous structure-less Lower Bolderberg Sands outcrop characterized by a fining upwards trend.

the Meuse gravels, and shows a few layers of finer material, and some oxidized patches with higher iron content. Within the white sand, hardly any structures are distinguishable.

This Genk member of the Bolderberg Sands clearly is one of the most homogeneous sediments studied. Comparable to the Mol and Kleine Nete point bar sands, the K range is less than one order of magnitude (Fig. 5). The K values (mean value of $10^{-3.9}$ m/s) are also comparable with those from the Kleine Nete and Mol Sands (respectively outcrop a and e) (Table 2). The experimental

| ID | -----Permeameter setup----- | | | ---Combination of boundary conditions--- | | | | Horizontal flow | |
	$\log_{10}(K_{xx})$	$\log_{10}(K_{zz})$	VANI	$\log_{10}(K_{xx})$	$\log_{10}(K_{zz})$	$\log_{10}(K_{xz})$	VANI	α_L (m)	α_{TV} (m)
b	-4.34**	-7.29**	890**	-	-	-	-	-	-
c	-4,15	-5,57	26,42	-4,16	-4,42	-9,66	1,82	2.7E+02*	4.3E-03*
d	-4,19	-4,19	1	-4,16	-4,24	-5,24	1,2	2,20E-01	3,50E-04
e	-3,64	-3,6	0,92	-3,68	-3,69	-5,37	1,03	3,50E-02	1,20E-04
f	-3,88	-5,31	26,71	-3,98	-4,79	-6,14	6,4	7.1E-01*	6.8E-04*
g	-4,8	-6,23	26,86	-4,86	-5,55	-12,59	4,97	2.4E+00*	1.9E-03*
h	-3,84	-4,02	1,51	-3,89	-3,97	-5,09	1,22	9,70E-02	8,00E-04
i	-	-6,05	-	-	-	-	-	-*	-*
j	-3,86	-3,85	0,98	-3,86	-3,87	-5,62	1,02	1,10E-01	1,00E-03
k	-4,13	-5,71	38,31	-4,05	-5,47	-13,08	26,46	3.7E+09*	2.1E-03*
l	-3,56	-3,88	2,08	-3,58	-3,77	-4,96	1,53	1,50E-01	1,40E-03
m	-4,06	-4,14	1,21	-4,09	-4,18	-12,23	1,22	7,90E-02	4,40E-04
n	-3,81	-3,84	1,07	-3,84	-3,86	-5,4	1,05	5,00E-02	3,50E-04
o	-3,86	-3,88	1,05	-3,9	-3,92	-8,61	1,04	2,60E-02	1,10E-04

* Presence of contrasting materials and structured heterogeneity, resulting in meaningless estimates of Fickian disper
** Calculated using arithmetic and harmonic means.

Table 3. Overview of calculated effective K values and dispersivities for the different grids presented in Figure 4.

variogram indicates the sampling grid was too small to capture the horizontal variability (no sill), while for the vertical direction the sill is reached after about 50 cm (Fig. 6, outcrop n). The entire measurement grid is used to calculate outcrop-scale parameter values in section 4.

Outcrop o: Bolderberg Sands at Maasmechelen (lower part)
The second Bolderberg Sands outcrop is even more homogeneous and shows no structures at all (Fig. 27). It is located only a few meters below the previous outcrop. Field observations indicated the sand at the top of the outcrop was finer than the sand below, explaining the trend in hydraulic conductivity.

The homogeneity is also clearly visible on the 10-cm spaced measurement grid (Fig. 4, outcrop o). As a result the $log_{10}(K)$ standard deviation is the overall smallest (0.15) across all outcrops (Table 2). The horizontal experimental variogram shows a pure nugget effect, but due to the trend in grain size the vertical variogram shows clear spatial correlation without a sill (Fig. 6, outcrop o). The entire measurement grid is used to calculate outcrop-scale parameter values in section 4.

4. Outcrop-scale effective *K* values and dispersivities

The effective *K* values obtained are listed in Table 3, both for the permeameter-type boundary conditions and the four alternative flow directions. The non-zero components of the *K* tensor are given together with the vertical anisotropy factor VANI.

The horizontal effective *K* values are all between $10^{-3.5}$ and $10^{-4.9}$ m/s. Hence, the variability of effective horizontal *K* within the studied outcrops of the Neogene aquifer remains limited. The vertical effective *K* values show more variations, ranging from $10^{-3.6}$ to $10^{-6.2}$ m/s. The relative differences between horizontal and vertical effective *K*, and between the different outcrops are consistent with our expectations based on *K* analysis on borehole cores (Beerten *et al.* 2010), but the Diest Clayey Top exhibits higher conductivities relative to the other outcrops than expected. The four combined fixed head boundary conditions gave similar results to those from the permeameter-type setups. The off-diagonal components of the *K* tensor are all at least one order of magnitude smaller than the diagonal components, which justifies the use of diagonal-tensor models like e.g. MODFLOW (Harbaugh, 2005) in the large-scale simulations of the Neogene aquifer (see Gedeon et al., 2011).

Concerning the calculated vertical anisotropy parameter VANI, we conclude that the Mol, Kasterlee and Bolderberg Sands remain isotropic at the scale of the numerical grid, while the Lommel Sands show a slight anisotropy with a maximum VANI of 1.20. For the Poederlee Sands (at Lichtaart), Diest Sands,
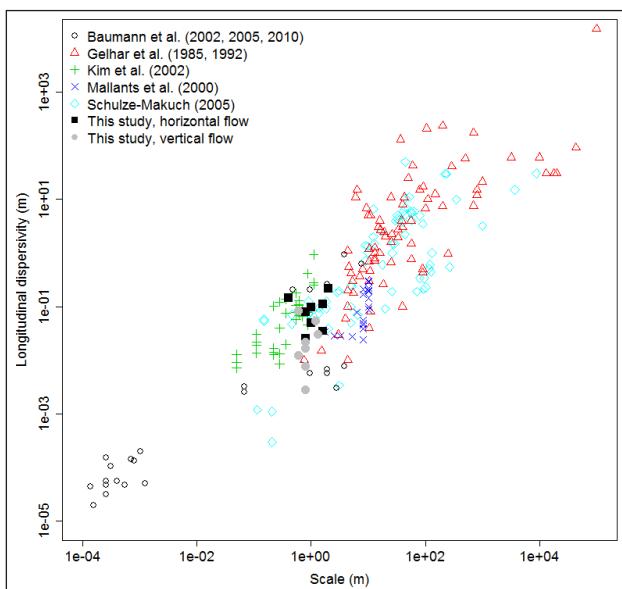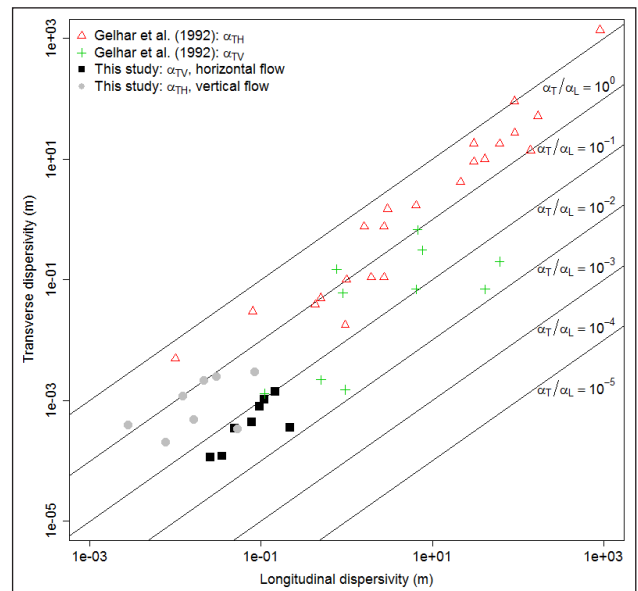

Figure 29. Numerically calculated longitudinal versus transverse dispersivity (both horizontal and vertical) for different flow directions combined with literature data from Gelhar et al. (1992).

and Diest Clayey Top outcrops, the VANI parameter is between 1.2 and 2. Higher values are obtained for the Kasterlee Clay, Poederlee Sands (at Kasterlee), and Campine Complex outcrop with frost structures, ranging from 26 to 40. Finally, the profile through the Campine Complex produces the overall highest value for VANI equal to 890.

PMPATH (included in Processing Modflow; Chiang and Kinzelback, 2001) was used to perform the particle tracking calculations. It uses a semi-analytical scheme (Pollock, 1988) and as input the simulation results from the flow model to calculate the groundwater paths and travel times. At the inflow boundary, 10 particles were inserted per grid cell to get a representative distribution.

The breakthrough curves of many of these particle tracking simulations show heavy tailing and multiple peaks (not shown). This indicates that a Fickian dispersion model (Bear, 1979) would not be appropriate for these geologic media, as this model has several shortcomings (Konikow, 2011), or that the representative elementary volumes of the studied sediments exceed the outcrop sizes. Nevertheless, dispersivities were estimated and the results presented in Table 3. The outcrops with distinctly different and contrasting materials with structured heterogeneity are marked with an asterisk, as their calculated dispersivities are very large and hence not meaningful. All other longitudinal dispersivities are between 10^{-3} and 10^0 m, and their transversal equivalents are one to three orders of magnitude smaller.

Fig. 28 shows the longitudinal dispersivity as a function of measurement scale. Only the meaningful values are included in the graph. Gelhar et al. (1985, 1992) and Schulze-Makuch (2005) collected published dispersivity data to estimate the scaling relationship. The work by Baumann et al. (2002, 2005, 2010) is focussed on pore-scale dispersion, and provides results that are in line with the macro-dispersion parameters obtained in the field. Kim et al. (2002) used TDR measurements to determine at the centimetre scale the longitudinal dispersivity in an unconfined sandy aquifer, which complements the previous two types of data sets. Finally, the natural gradient tracer study by Mallants et al. (2000) provided several dispersivity values for the Brasschaat and Mol Sands of the Neogene aquifer; such field-based values are useful in a comparison with the numerically calculated values from the present study.

Based on Fig. 29 all available data display a high degree of consistency with the observed scatter being representative of different degrees of sediment heterogeneity. The values we obtained with this fairly simple dispersivity calculation approach are consistent with the literature data. The four outliers in Table 3 are the Kasterlee Clay, the Campine Complex frost structures

Figure 28. Longitudinal dispersivity as a function of measurement scale. Literature values are combined with numerically calculated values for outcrops. Data from Mallants et al. (2000) was also obtained from Neogene aquifer sediments.

outcrop, and both Poederlee outcrops at Kasterlee. Because of the highly contrasting lithologies in these outcrops, a dual domain approach (e.g. Flach et al., 2004) might be more appropriate. The Mol and Bolderberg Sand outcrops show the lowest dispersivity values, although a difference of about one order of magnitude exists between the values obtained from considering horizontal and vertical flow directions; this indicates that at least an anisotropic dispersion model should be used. These low dispersivity values also accord most with the data obtained from similar sediments by Mallants et al. (2000).

Vertical and horizontal transverse dispersivities are shown in Fig. 29, again without the outliers from Table 3. The data from Gelhar et al. (1992) shows α_L/α_T ratios between 1 and 100 for the horizontal transverse dispersivity (α_{TH}), and up to 1000 for the vertical one (α_{TV}). This is consistent with our data, although the effect of flow direction (i.e. horizontal versus vertical) on the α_L/α_T ratios is clearly visible.

These analyses of dispersivities demonstrate that the use of isotropic dispersion coefficients in such highly stratified sediments may not yield correct results; approaches that account for effects of layering on dispersion are preferred. For the few sediments with highly contrasting materials and structured heterogeneity more complex approaches are recommended (such as dual domain approaches or more explicit representation of the small-scale heterogeneity instead of using a macro-description).

5. Conclusions

Air permeameter measurements are an efficient and flexible way to characterize hydraulic properties of outcropping sediments. Investigations on different lithologies, vertical profiles, or even two-dimensional regular grids are generally straightforward. Besides effectively characterizing hydraulic conductivity and its small-scale spatial variability, numerical methods can be used in conjunction to derive an effective K tensor at the scale of the entire outcrop, as well as the dispersivity transport parameter.

The geometric mean air permeameter based K values for the outcrops discussed in this paper range from $10^{-5.94}$ m/s to $10^{-3.68}$ m/s, whereas the minimum and maximum of the individual measurements amounted respectively to $10^{-9.17}$ and $10^{-1.56}$ m/s. The maximum difference between values obtained for one outcrop ranged from less than one order of magnitude to more than four orders of magnitude, indicating the presence of important small-scale heterogeneities as well as several very homogeneous outcrops.

Investigating spatial correlation for the different measurement grids showed that, at the considered outcrop scales, hardly any correlation exists for several formations (e.g. e, Mol Sands; g, bottom of Poederlee Fm.; j, Kasterlee Sands), while others display a significant increase of the variability (i.e. variance) with distance (e.g. i, Poederlee-Kasterlee transition zone; k, Kasterlee Clay; l, Diest Clayey Top; m, Diest Sands; n, Bolderberg Sands). Most horizontal experimental variograms do not reach the semivariance values of the corresponding vertical ones, which may indicate that the horizontal outcrop extents are only a fraction of the true horizontal correlation lengths, or, for a layered outcrop, that the variability within a layer is lower than variability across layers. Moreover, the contrasts in heterogeneity between the different formations are very well illustrated by means of the experimental variograms.

The grain size based K predictions confirmed the systematic offset between similar outcropping and subsurface sediments as discussed by Rogiers et al. (2013a). The offset seems to be larger for the more clayey sediments that are also more affected by weathering. For recently excavated outcrops, with still several meters of overburden, the bias between grain size and air permeameter based predictions seemed to be negligible. Moreover, the discrepancies between K measurements and predictions based on the non-linear site-specific GLUE-ANN model (Rogiers et al., 2012) revealed that the discrepancies are highest where fine silt fractions exist in outcrop lithologies, a result of such textural fractions not occurring in the borehole data on which the model was trained. The finer textures in some of the outcrops may originate from disintegration of glauconite particles by weathering.

The numerically upscaled effective K values obtained for the different outcrops range from $10^{-4.9}$ m/s to $10^{-3.6}$ m/s in the horizontal direction and from $10^{-6.2}$ m/s to $10^{-3.6}$ m/s in the vertical direction. The corresponding vertical anisotropy values range between 1 and 40. Most of the calculated longitudinal dispersivities fit well within literature data, given the scale of the outcrops. A few outliers were obtained for outcrops with contrasting lithologies, where a dual domain approach might be more appropriate. The ratio between longitudinal and transverse dispersivities seems to be rather high, but falls in the range reported in literature. Moreover, the dispersivity values obtained by Mallants et al. (2000) at a slightly larger scale are very similar. This builds confidence for the use of numerically calculated dispersivity values from outcrop sediments within larger-scale contaminant transport models.

Increasing size and number of investigated outcrops of the same formations would provide more information on the larger-scale variability. A systematic study addressing K-dependency on sediment porosity, density, compaction and weathering processes might provide adequate tools to convert the outcrop K-data into effective values for subsurface groundwater flow and contaminant transport simulation.

References

AMINAL, 2003. De Kleine Nete en de Aa - Naar een ecologisch herstel van waterloop en vallei (p. 26). Afdeling Water, Brussel.

Baumann, T., Müller, S. & Niessner, R., 2002. Migration of dissolved heavy metal compounds and PCP in the presence of colloids through a heterogeneous calcareous gravel and a homogeneous quartz sand – pilot scale experiments. Water Research, 36, 1213–1223.

Baumann, T. & Werth, C.J., 2005. Visualization of colloid transport through heterogeneous porous media using magnetic resonance imaging. Colloids and Surfaces A: Physicochemical and Engineering Aspects, 265, 2–10.

Baumann, T., Toops, L. & Niessner, R., 2010. Colloid dispersion on the pore scale. Water Research, 44(4), 1246-54.

Bear, J., 1979. Hydraulics of Groundwater, 569. New York: McGraw-Hill.

Beerten, K., 2006. Toelichting bij de Quartairgeologische kaart, kaartblad 17 Mol. Vlaamse Overheid, Dienst Natuurlijke Rijkdommen.

Beerten, K., 2010. Geomorphological evolution of the Nete basin: identification of past events to assess the future evolution. SCK•CEN external report (p. 41). Mol.

Beerten, K., Wemaere, I., Gedeon, M., Labat, S., Rogiers, B., Mallants, D., Salah, S. & Leterme, B., 2010. Geological, hydrogeological and hydrological data for the Dessel disposal site. Project near surface disposal of category A waste at Dessel – Version 1.- Brussels, Belgium: NIRAS/ONDRAF, 2010.- 273 p.- NIROND–TR 2009–05 E V1.

Chiang, W. & Kinzelbach, W., 2001. 3D-groundwater modeling with PMWIN. Springer, Berlin. ISBN 3-540- 67744-5

Coetsiers, M. & Walraevens, K., 2006. Chemical characterization of the Neogene Aquifer, Belgium. Hydrogeology Journal 14, 1556-1568.

Coetsiers, M., Blaser, P., Martens, K. & Walraevens, K., 2008. Natural background levels and threshold values for groundwater in fluvial Pleistocene and Tertiary marine aquifers in Flanders, Belgium. Environmental Geology, 57(5), 1155-1168.

De Bie, E., Martens, K., Haesevoets, A. & Florus, M., 2007. Rivierherstel van de Kleine Nete tussen Herentals en Kasterlee. Water, Congres Watersysteemkennis 2006-2007, Bodem, Grondwater en Ecosysteem (pp. 1-5).

De Marsily, G., Delay, F., Goncalves, J., Renard, P., Teles, V. & Violette, S., 2005. Dealing with spatial heterogeneity. Hydrogeology Journal, 13(1), 161–183.

Flach, G. P., Crisman, S.A. & Molz, F. J., 2004. Comparison of single-domain and dual-domain subsurface transport models. Ground Water, 42(6-7), 815–28.

Fobe, B., 1995. Litologie en litostratigrafie van de Formatie van Kasterlee (Plioceen van de Kempen). Natuurwetenschappelijk Tijdschrift, 75(2), 35-45.

Gedeon, M., Wemaere, I. & Marivoet, J., 2007. Regional groundwater model of north-east Belgium. Journal of Hydrology, 335(1-2), 133-139.

Gedeon, M., 2008. Neogene Aquifer Model.- Mol, Belgium: SCK•CEN, 2008.- 110 p.- (External Report of the Belgian Nuclear Research Centre; ER-48; CCHO-2004-2470/00/00, DS 251-A51).- ISSN 1782-2335

Gedeon, M., Mallants, D., Vandersteen, K. & Rogiers, B., 2011. Hydrogeological modelling of the Dessel site - Overview report. Project near surface disposal of category A waste at Dessel. NIROND-TR report 2008–15 E V2

Gedeon, M., & Mallants, D., 2012. Sensitivity Analysis of a Combined Groundwater Flow and Solute Transport Model Using Local-Grid Refinement: A Case Study. Mathematical Geosciences, 44(7), 881-899.

Gelhar, L.W., Mantoglou, A., Welty, C. & Rehfeldt, K.R., 1985. A review of field-scale physical solute transport processes in saturated and unsaturated porous media. Palo Alto, California: Electric Power Research Institute EPRI EA-4190 Project 2485–5.

Gelhar, L.W., Welty, C. & Rehfeldt, K., 1992. A Critical Review of Data on Field-Scale Dispersion in Aquifers. Water Resources Research, 28(7), 1955-1974.

Gullentops, F. & Wouters, L. (Eds.), 1996. Delfstoffen in Vlaanderen. Ministerie Vlaamse Gemeenschap, Brussel, 198pp.

Gullentops, F., Bogemans, F., De Moor, G., Paulissen, E. & Pissart, A., 2001. Quaternary lithostratigraphic units (Belgium). Geologica Belgica, 4(1-2), 153–164.

Harbaugh, A.W., 2005. MODFLOW-2005, The U.S. Geological Survey modular ground-water model—the Ground-Water Flow Process: U.S. Geological Survey Techniques and Methods 6-A16, USGS, 2005

Huysmans, M., Peeters, L., Moermans, G. & Dassargues, A., 2008. Relating small-scale sedimentary structures and permeability in a cross-bedded aquifer. Journal of Hydrology, 361(1-2), 41-51.

Huysmans, M. & Dassargues, A., 2009. Application of multiple-point geostatistics on modelling groundwater flow and transport in a cross-bedded aquifer (Belgium). Hydrogeology Journal, 17(8), 1901–1911.

Iversen, B.V., Moldrup, P., Schjonning, P. & Jacobsen, O.H., 2003. Field Application of a Portable Air Permeameter to Characterize Spatial Variability in Air and Water Permeability. Vadose Zone Journal, 2(4), 618-626.

Jacques, D., Leterme, B., Beerten, K., Schneider, S., Finke, P. & Mallants, D., 2010. Long-term evolution of the multi-layer cover. Project near surface disposal of category A waste at Dessel. NIROND-TR 2010-03 E, September 2010.

Kim, D.-J., Kim, J.-S., Yun, S.-T. & Lee, S.-H., 2002. Determination of longitudinal dispersivity in an unconfined sandy aquifer. Hydrological Processes, 16(10), 1955–1964.

Koltermann, C. & Gorelick, S., 1996. Heterogeneity in Sedimentary Deposits: A Review of Structure Imitating, Process Imitating, and Descriptive Approaches. Water Resources Research, 32(9), 2617-2658.

Konikow, L.F., 2011. The secret to successful solute-transport modeling. Ground Water, 49(2), 144-59.

Laga, P., Louwye, S. & Geets, S., 2001. Paleogene and Neogene lithostratigraphic units (Belgium). Geologica Belgica, 4(1-2), 135–152.

Li, L., Zhou, H. & Jaime Gómez-Hernández, J., 2011. A Comparative Study of Three-Dimensional Hydraulic Conductivity Upscaling at the MAcro-Dispersion Experiment (MADE) site, Columbus Air Force Base, Mississippi (USA). Journal of Hydrology, 404(3-4), 278-293.

Louwye, S., De Schepper, S., Laga, P. & Vandenberghe, N., 2007. The Upper Miocene of the southern North Sea Basin (northern Belgium): a palaeoenvironmental and stratigraphical reconstruction using dinoflagellate cysts. Geological Magazine, 144(1), 33.

Louwye, S. & Laga, P., 2008. Dinoflagellate cyst stratigraphy and palaeoenvironment of the marginal marine Middle and Upper Miocene of the eastern Campine area, northern Belgium (southern North Sea Basin). Geological Journal, 43(1), 75–94.

Louwye, S. & De Schepper, S., 2010. The Miocene–Pliocene hiatus in the southern North Sea Basin (northern Belgium) revealed by dinoflagellate cysts. Geological Magazine, 147(05), 760-776.

Mallants, D., Espino, A., Hoorick, M., Feyen, J., Vandenberghe, N. & Loy, W., 2000. Dispersivity estimates from a tracer experiment in a sandy aquifer. Ground Water, 38(2), 304–310.

Meyus, Y., Batelaan, O. & De Smedt, F., 2000. Concept Vlaams Grondwater Model (VGM). Deelrapport: Technisch concept van het VGM: Hydrogeologische Codering van de Ondergrond van Vlaanderen (HCOV). (p. 58). Brussel.

New England Research & Vindum Engineering, 2011. TinyPerm II Portable Air Permeameter, User's Manual. Retrieved from http://www.vindum.com/TinyPermManual.pdf on 14-06-2011.

ONDRAF/NIRAS, 2010. Het cAt-project in Dessel. Een langetermijnoplossing voor het Belgische categorie A-afval. Retrieved from http://www.niras-cat.be/downloads/cAt_masterplan_NL_LOW.pdf on 07-12-2011.

Patyn, J., Ledoux, E., & Bonne, A., 1989. Geohydrological research in relation to radioactive waste disposal in an argillaceous formation. Journal of Hydrology 109:267–285.

Pollock, D.W., 1988. Semianalytical Computation of Path Lines for Finite-Difference Models. Ground Water, 26(6), 743-750.

Possemiers, M., Huysmans, M., Peeters, L., Batelaan, O. & Dassargues, A., 2012. Relationship between sedimentary features and permeability at different scales in the Brussels Sands. Geologica Belgica, 15(3), 156-164.

Rogiers, B., Schiltz, M., Beerten, K., Gedeon, M., Mallants, D., Batelaan, O., Dassargues, A. & Huysmans, M., 2010a. Groundwater model parameter identification using a combination of cone-penetration tests and borehole data. IAHR international groundwater symposium (p. 19). Valencia.

Rogiers, B., Mallants, D., Batelaan, O., Gedeon, M., Huysmans, M. & Dassargues, A., 2010b. Caractérisation de l'hétérogénéité de la conductivité hydraulique à saturation au moyen d'essais de pénétration au cône. 35 èmes journées scientifiques du Groupe Francophone d'Humidimétrie et des TraNsferts en Milieux Poreux: Transferts en milieux poreux : Hétérogénéité des processus et des propriétés, GFHN 2010, Bulletin du G.F.H.N. N°56: 149-150. Louvain-la-Neuve, 23-25 November 2010. - ISSN: 0997 - 1076

Rogiers, B., Mallants, D., Batelaan, O., Gedeon, M., Huysmans, M. & Dassargues, A., 2010c. Geostatistical analysis of primary and secondary data in a sandy aquifer at Mol/Dessel, Belgium. 8th International conference on Geostatistics for Environmental Applications, geoENV 2010, Gent, 13-15 September 2010.

Rogiers, B., Mallants, D., Batelaan, O.,Gedeon, M., Huysmans, M. & Dassargues, A., 2010d. Exploratory and structural data analysis of a sandy aquifer at Mol/Dessel, Belgium. Geophysical Research Abstracts, Vol. 12, EGU General Assembly 2010, Vienna, 3-7 May 2010.

Rogiers, B., Beerten, K., Smekens, T. & Mallants, D., 2011. Air permeability measurements on Neogene and Quaternary sediments from the Campine area: using outcrop analogues for determining hydrodynamic aquifer properties. SCK•CEN ER-177 (p. 23). Mol.

Rogiers, B., Mallants, D., Batelaan, O., Gedeon, M., Huysmans, M. & Dassargues, A., 2012. Estimation of hydraulic conductivity and its uncertainty from grain size data using GLUE and artificial neural networks. Mathematical Geosciences, 44, 739–763.

Rogiers, B., Beerten, K., Smeekens, T., Mallants, D., Gedeon, M., Huysmans, M., Batelaan, O. & Dassargues, A., 2013a. The usefulness of outcrop analogue air permeameter measurements for analysing aquifer heterogeneity: Quantifying outcrop hydraulic conductivity and its spatial variability. Hydrological Processes, in review.

Rogiers, B., Beerten, K., Smeekens, T., Mallants, D., Gedeon, M., Huysmans, M., Batelaan, O. & Dassargues, A., 2013b. The usefulness of outcrop analogue air permeameter measurements for analysing aquifer heterogeneity: Testing outcrop hydrogeological parameters with independent borehole data. Submitted to Hydrology and Earth System Sciences.

Ronayne, M.J., Gorelick, S.M. & Zheng, C., 2010. Geological modeling of submeter scale heterogeneity and its influence on tracer transport in a fluvial aquifer. Water Resources Research, 46(10), 1-9.

Salamon, P., Fernàndez-Garcia, D. & Gómez-Hernández, J.J., 2006. A review and numerical assessment of the random walk particle tracking method. Journal of Contaminant Hydrology, 87(3-4), 277-305.

Schaap, M., Leij, F. & Van Genuchten, M.Th., 2001. Rosetta: A computer program for estimating soil hydraulic parameters with hierarchical pedotransfer functions. Journal of Hydrology 251(3–4):163–176.

Schulze-Makuch, D., 2005. Longitudinal dispersivity data and implications for scaling behavior. Ground Water, 43(3), 443–456.

Sibelco, 2010. Silica sand of Mol. Technical Datasheet TDS.03.05.10 2010-12-09

Seuntjens, P., Mallants, D., Simunek, J., Patyn, J. & Jacques, D., 2002. Sensitivity analysis of physical and chemical properties affecting field-scale cadmium transport in a heterogeneous soil profile. Journal of Hydrology, 264(1-4), 185-202.

Van Camp, M., Coetsiers, M., Martens, K. & Walraevens, K., 2010. Effects of multi-annual climate variability on the hydrodynamic evolution (1833-present) in a shallow aquifer system in northern Belgium. Hydrological Sciences Journal 55(5), 763-779.

Van Camp, M., Martens, K., & Walraevens, K. (2012). Impact of recent climate variability on an aquifer system in north Belgium The Netherlands Campine Cuesta Nete Basin Campine Plateau. Geologica Belgica, 15(1-2), 73–80.

Vandenberghe, N., Van Simaeys, S., Steurbaut, E., Jagt, J.W.M. & Felder, P.J., 2004. Stratigraphic architecture of the Upper Cretaceous and Cenozoic along the southern border of the North Sea Basin in Belgium. Netherlands Journal of Geosciences 83, 155-171.

Vienken, T. & Dietrich, P., 2011. Field evaluation of methods for determining hydraulic conductivity from grain size data. Journal of Hydrology, 400(1-2), 58-71.

VMM, 2005. Grondwaterbeheer in Vlaanderen: het onzichtbare water doorgrond. Bijlage 4: Vergunde debieten per grondwaterlichaam. Retrieved from http://www.vmm.be/water/toestand-watersystemen/ watersysteemkennis/watersysteemkennis-grondwater/rapporten-grondwaterbeheer-in-vlaanderen-het-onzichtbare-water-doorgrond on 21-02-2012.

VMM, 2008. Het Centraal Kempisch Systeem (p. 108).

Wouters, L. & Vandenberghe, N., 1994. Geologie van de Kempen. Niras: Brussel.

Yu, L., Rogiers, B., Gedeon, M., Wemaere, I., Marivoet, J., De Craen, M. & Mallants, D., 2012. A critical review of laboratory and in-situ hydraulic conductivity measurements for the Boom Clay in Belgium. Applied Clay Science, 75-76: 1-12.

Running title droit

Running title gauche